JACS
JOURNAL OF THE AMERICAN CHEMICAL SOCIETY

pubs.acs.org/JACS

Article

Protein Matrix Control of Reaction Center Excitation in Photosystem II

Abhishek Sirohiwal, Frank Neese, and Dimitrios A. Pantazis*

Cite This: J. Am. Chem. Soc. 2020, 142, 18174−18190

Read Online

ACCESS | Metrics & More | Article Recommendations | Supporting Information

ABSTRACT: Photosystem II (PSII) is a multisubunit pigment−protein complex that uses light-induced charge separation to power oxygenic photosynthesis. Its reaction center chromophores, where the charge transfer cascade is initiated, are arranged symmetrically along the D1 and D2 core polypeptides and comprise four chlorophyll (P_{D1}, P_{D2}, Chl_{D1}, Chl_{D2}) and two pheophytin molecules ($Pheo_{D1}$ and $Pheo_{D2}$). Evolution favored productive electron transfer only via the D1 branch, with the precise nature of primary excitation and the factors that control asymmetric charge transfer remaining under investigation. Here we present a detailed atomistic description for both. We combine large-scale simulations of membrane-embedded PSII with high-level quantum-mechanics/molecular-mechanics (QM/MM) calculations of individual and coupled reaction center chromophores to describe reaction center excited states. We employ both range-separated time-dependent density functional theory and the recently developed domain based local pair natural orbital (DLPNO) implementation of the similarity transformed equation of motion coupled cluster theory with single and double excitations (STEOM-CCSD), the first coupled cluster QM/MM calculations of the reaction center. We find that the protein matrix is exclusively responsible for both transverse (chlorophylls versus pheophytins) and lateral (D1 versus D2 branch) excitation asymmetry, making Chl_{D1} the chromophore with the lowest site energy. Multipigment calculations show that the protein matrix renders the $Chl_{D1} \rightarrow Pheo_{D1}$ charge-transfer the lowest energy excitation globally within the reaction center, lower than any pigment-centered local excitation. Remarkably, no low-energy charge transfer states are located within the "special pair" P_{D1}−P_{D2}, which is therefore excluded as the site of initial charge separation in PSII. Finally, molecular dynamics simulations suggest that modulation of the electrostatic environment due to protein conformational flexibility enables direct excitation of low-lying charge transfer states by far-red light.

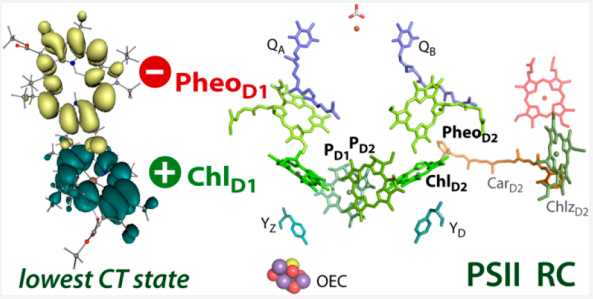

1. INTRODUCTION

Photosystem II (PSII) is a dimeric multisubunit protein−pigment complex responsible for the light-driven oxidation of water into molecular oxygen and for the supply of reducing equivalents in oxygenic photosynthesis.[1−7] Excitation-induced charge separation and the early steps of the electron transfer cascade take place within a cluster of six chlorin molecules known as the reaction center (RC). The RC comprises four chlorophylls (typically chlorophyll *a*), the central P_{D1} and P_{D2} "special" pair flanked by chlorophylls Chl_{D1} and Chl_{D2}, and two pheophytin molecules, $Pheo_{D1}$ and $Pheo_{D2}$. The RC chromophores are arranged in a symmetric fashion along the D1 and D2 protein subunits of PSII (Figure 1) that are highly conserved across oxygenic photosynthetic organisms. The RC of PSII receives excitation energy from integral chlorophyll-rich polypeptides (CP43 and CP47) and from external light-harvesting antenna systems that vary among different species.

Following excitation and charge separation within the RC chromophores, the radical anion is localized within 0.3−3 ps[8−12] on $Pheo_{D1}$ and the hole is distributed over the P_{D1}/P_{D2} pair.[13−15] The resulting radical cation, known as $P680^+$, is the strongest oxidant in biology. With an estimated reduction potential of 1.1−1.3 V, $P680^+$ is able to drive the oxidation of water at the oxygen-evolving complex (OEC) via a redox active tyrosine residue (Tyr161 or Y_Z) that interfaces the two sites. A distinctive feature of PSII is the utilization of the D1 branch, which also harbors the OEC, for electron transfer following productive charge separation. On the acceptor side the negative charge proceeds from $Pheo_{D1}$ to plastoquinone Q_A and finally to the terminal mobile electron acceptor plastoquinone Q_B.[16]

Key questions include the nature and localization of initial excited states, the nature and energetics of charge-transfer (CT) excited states that may lead to productive charge separation, and the factors that determine the asymmetry of RC chromophores and directionality of electron transfer.[13,17,18]

Received: August 8, 2020
Published: October 9, 2020

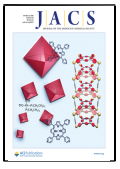

https://dx.doi.org/10.1021/jacs.0c08526
J. Am. Chem. Soc. 2020, 142, 18174−18190

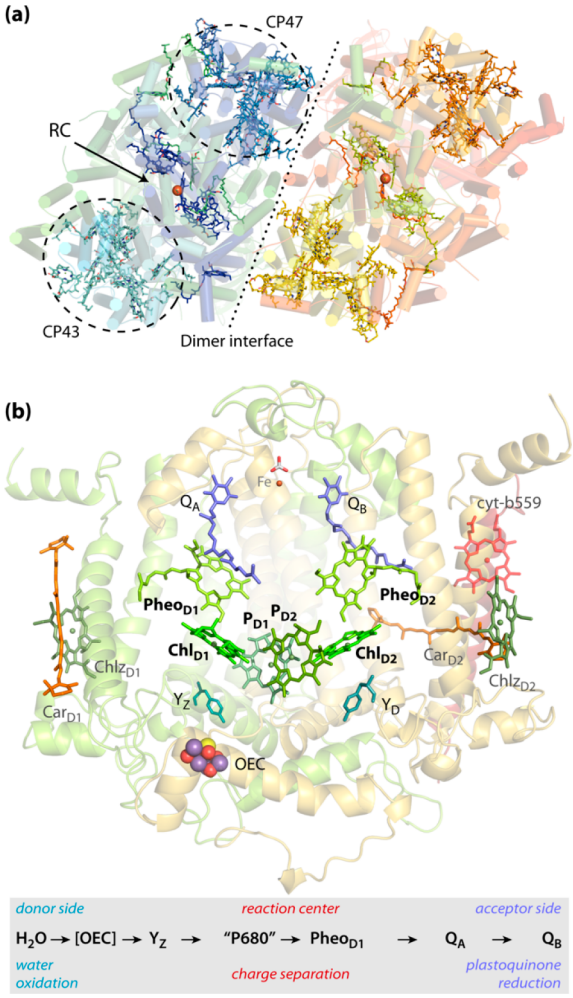

Figure 1. (a) Arrangement of the photosystem II dimer viewed from the stromal side of the membrane; marked regions are the core-antenna chlorophyll proteins CP43 and CP47, and the reaction center. (b) Reaction center chromophores and selected additional components within the D1 and D2 polypeptides, with a scheme indicating the flow of electrons within PSII.

The multimer model[19] assumes that the local excitation energies of all pigments are similar, thus favoring delocalized excitation, but other studies supported models where the chromophore energies are distinct.[12,20−23] The P_{D1}−P_{D2} pair is a prime candidate for the initial excitation event in analogy to the "special pair" of bacterial reaction centers.[24,25] One of two major charge-transfer pathways[26,27] considered includes excitation and charge separation within this pair: $[P_{D1}P_{D2}]^* \rightarrow P_{D1}^-P_{D2}^+$, and the negative charge is subsequently transferred to Chl_{D1}, i.e., $[P_{D1}P_{D2}]^+Chl_{D1}^-$,[28−30] before proceeding to $Pheo_{D1}$. However, the prevailing view is that Chl_{D1} is the most red-shifted pigment and hence may function as the primary electron donor[11,21,23,31,32] (uncertainties remain regarding the low-energy excited states of pheophytins[23,33−35]). The second pathway is thus described as $[Chl_{D1}Pheo_{D1}]^* \rightarrow Chl_{D1}^+Pheo_{D1}^-$. It has been proposed that room temperature structural perturbation in the protein can induce switching between the different pathways.[26] Both would eventually lead to the same $P_{D1}^+Pheo_{D1}^-$ charge-separated state, but the electronic nature of the excitation and all underlying events are fundamentally distinct.

Stark spectroscopy studies suggested the presence of mixed local excitation−charge-transfer excitation in the active D1 branch,[36,37] while Styring and co-workers[38−40] proposed the presence of low-energy CT states responsible for far-red charge-separation and furthermore that the photochemistry of PSII is wavelength-dependent.[39] An important fact is that although the working threshold of PSII is typically considered to be 680 nm, charge separation in the reaction center can be initiated with far-red light (700−780 nm) either by direct excitation of a low-lying charge transfer state in Chl *a* RCs or by excitation of far-red chlorophylls (Chl *d* and *f*).[38,39,41−50] These observations highlight the significance of low-energy charge-transfer states for RC function.[17] Remarkably, no quantum chemical study has so far identified interpigment CT excited states low enough in energy to be consistent with these observations.

It is useful to keep in mind that experimental studies are typically restricted to nonphysiological and perhaps nonfunctional PSII preparations that may yield varying observations depending on the type of preparation and conditions used. Even disregarding light-harvesting antennae, a PSII monomer comprises more than 20 proteins and dozens of chlorophylls. Core complex preparations (PSII-CC) reduce this complexity by maintaining only the D1, D2, Cytochrome b_{559}, CP43, and CP47 proteins, but the study of RC would still be challenging due to spectral congestion by the core protein chlorophylls,[27] therefore most experimental work involves PSII "RC complexes" (PSII-RCC) that maintain D1, D2, and Cytochrome b_{559}.[51−55] These are considered as a minimal structural scaffold for studying the RC,[26,27,33,56−58] but their actual structure and the extent to which they represent the physiological system are debatable.[48,59−61] Computational studies can potentially assist in bridging the gap between observations made on such preparations and the properties of physiological PSII.

Theoretical studies[14,15,23,62−82] of photosynthetic reaction centers are challenging due to the size and complexity of the system. Beyond site energies, detailed electronic structure analysis of excited states that may be delocalized among different chromophores necessitates the use of quantum chemical approaches. A landmark study by Frankcombe used time-dependent density functional theory (TD-DFT) for the excited states of all PSII RC chromophores in the absence of the protein environment.[62] This and subsequent similar studies find neither asymmetry in local excitations along the D1 and D2 branches, nor low-lying CT states that could be related to the charge-separation function of the RC.[62,65] Taking the protein matrix into account with a combined quantum−mechanics/molecular−mechanics approach (QM/MM)[83−85] is obviously necessary. However, this approach must not be viewed as a mere technical extension that can automatically deliver good results. Four distinct methodological requirements must be met simultaneously and successfully to ensure a meaningful and reliable outcome. These are (i) explicit atomistic representation of the complete protein matrix, potentially with consideration of conformational dynamics, (ii) high-quality quantum chemical geometric definition of the chromophores[86−89] as opposed to the direct use of crystallographic coordinates, (iii) reliable excited state calculations of single *and* coupled chromophores, because site energies alone are insufficient to address the electronic nature of multi-chromophore excitations, and (iv) high-level quantum chemical methods that ensure the correct response of excited

https://dx.doi.org/10.1021/jacs.0c08526
J. Am. Chem. Soc. 2020, 142, 18174−18190

state energetics to protein electrostatics and, above all, provide a reliable description of the nature and energetics of interpigment charge-transfer excited states. The present study addresses for the first time all of the above requirements in a definitive way, aiming to provide reliable quantitative insights into the excitation profile of the reaction center of PSII.

A large-scale model of an entire membrane-embedded PSII complex is used as the basis for multiscale QM/MM modeling on geometry-optimized pigments to uncover the influence of the protein environment on the excitation profile of reaction center chromophores. Highly accurate quantum chemical descriptions of both local and distributed excitations among pairs of chromophores are obtained by long-range corrected time-dependent DFT as well as by coupled cluster theory at a level employed for the first time in such simulations, namely the similarity transformed equation of motion coupled cluster theory with single and double excitations (STEOM-CCSD). Our results provide a complete view of the nature and energetics of local and, most importantly, of charge-transfer excitations among different chromophore pairs. The results explain the origin of the dual type of asymmetry in the RC and identify the pigment pair responsible for the primary charge transfer excitation. In combination with insights from molecular dynamics simulations we determine the static and dynamic factors that control the excitation profile of the reaction center and enable charge separation to occur with far-red light.

2. METHODOLOGY

2.1. Preparation of Models. The lipid-bilayer embedded model of Photosystem II is based on the high-resolution dimeric crystal structure (1.9 Å) of *Thermosynechococcus vulcanus* (PDB ID: 3WU2).[5] In the present work, we have used one of the monomers to build the entire system. Missing structural elements were completed to reproduce the physiological intactness of the complex. All crystallographic water associated with the monomer was retained and additional water molecules were added using the 3D-RISM technique[90−94] (three-dimensional reference interaction site model) to achieve a physiological hydration state of the protein complex. The PSII monomer was embedded inside a POPC (1-palmitoyl-2-oleoyl-*sn*-glycero-3-phosphocholine) lipid bilayer of dimension 176 × 176 Å^2 using *Packmol-Memgen*.[95,96] A total of 784 POPC molecules were added in the upper and lower leaflets of the trans-membrane region. The membrane-embedded protein complex was placed inside a water box. Appropriate amounts of Na^+ and Cl^- ions were added to neutralize the system and maintain a physiological concentration of 0.15 M. The complete dimensions of the system were 176 × 176 × 160 Å^3 and it consists of 512 341 atoms. (Figure 2).

The electrostatic charges for all the cofactors were computed based on the MK-RESP (Merz−Kollman Restrained Electrostatic Potential) methodology.[97,98] For the organic cofactors, first the hydrogens atoms were optimized at the B3LYP/Def2-SVP level[99,100] and then single-point calculations were performed at the HF/6-31G* level of theory[97,101,102] using the ORCA program[103] and RESP fitting of the charges was performed using the Multiwfn code.[104] A bonded model is employed for the computation of the RESP charges on the OEC (Mn_4CaO_5- Oxygen Evolving Complex) and NHI (nonheme iron) sites, as a first step, a small cluster model is built around metal sites including the side chain of the residues which form a direct coordination with the metal site. The OEC is modeled in its S_1 state of the Kok−Joliot cycle, i.e., the oxidation states are Mn1(III)−Mn2(IV)−Mn3(IV)−Mn4(III) and involved ligands are Asp170, Glu354, Ala344, Asp342, Glu189, His332, Glu333, and four H_2O molecules. Similarly, the NHI site is modeled as Fe(II) with the ligands HCO_3^-, His214, His268, His215, and His272. These models were first optimized at B3LYP/Def2-TZVP and then RESP fitting is performed at B3LYP/6-31G* level. More importantly, we restrained the charge of the backbone atoms of the residues according to the original AMBER force field[102] as such a procedure is known to produce better backbone dynamics during the simulation.[105] The RESP charges of the chlorophylls and the heme iron site were calculated in a similar fashion. The chlorophylls and the heme-iron are ligated axially to amino acids and water molecules, wherever applicable. For example, P_{D1} and P_{D2} of the reaction center are axially ligated to histidine residues and Chl_{D1} and Chl_{D2} are axially ligated to a single water molecule. Similarly, both heme sites are bound axially with two histidine residues.

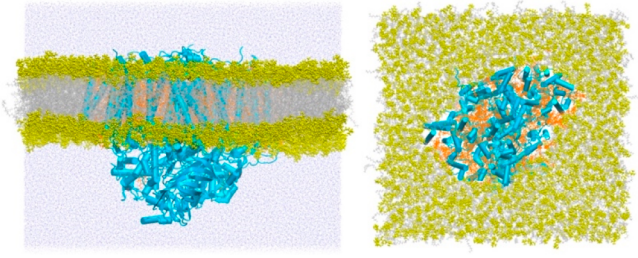

Figure 2. Side and top (stromal) view of the molecular mechanics model of the PSII monomer embedded in an equilibrated POPC lipid bilayer. The simulation box has dimensions of 176 × 176 × 160 Å^3.

Bonded parameters for the chlorophyll *a*,[106] heme,[107] and nonheme iron site[108] were obtained from the literature. Custom bonded parameters were defined for the OEC based on the study by Guerra et al.[109] Parameters for the standard protein residues were described using the Amber14SB force field.[110] The TIP3P model[111] was chosen for the water. The bonded parameters for the organic cofactors were described with GAFF2.[112] The LIPID17 force field[113,114] was chosen to describe our POPC bilayer. The nonbonded parameters for the metal ions were based on their respective oxidation states using data sets[105,115,116] available for the TIP3P water model. For Na^+ and Cl^-, we used the Joung−Cheatham parameters compatible with the TIP3P water model.[117,118]

2.2. Classical Molecular Dynamics Simulations. The complete system was minimized systematically to remove unfavorable geometric clashes. During the equilibration phase, the system is slowly heated from 10 to 100 K during 5 ps in the NVT ensemble. In the next step, the temperature is slowly increased from 100 to 303 K in the NPT ensemble, while maintaining the positional restraints (20 kcal mol^{-1} Å^{-2}) on the C_α atoms of amino acids. The temperature during this procedure is controlled using the Langevin dynamics[119] with a collision frequency of 5 ps^{-1}. We released the restraints on C_α atoms in a controlled fashion (2 kcal mol^{-1} Å^{-2}/400 ps) and subsequently invoked the Monte Carlo/Molecular Dynamics (MC/MD) module[120] for a controlled hydration and dehydration from bulk to protein, and vice versa. The system was then further equilibrated for another 63 ns in the NPT ensemble to properly equilibrate the lipid bilayer. Thereafter, we initiated the production simulation for 12 ns in the NPT ensemble using the collision frequency (Langevin dynamics) of 1 ps^{-1}. The pressure was regulated anisotropically using the Berendsen barostat[121] with a relaxation time of 2 ps and maintained at 1 bar. Particle Mesh Ewald (PME)[122] approach is used to treat all electrostatic interactions with a 10 Å cutoff. The SHAKE algorithm[123] was used to constrain bonds involving hydrogen atoms, which allowed us to use a time step of 2 fs. The frames were saved every 2 ps. Minimizations were performed using the CPU version while equilibration and production simulations were performed using the GPU version of the *pmemd* engine[124−126] of the AMBER18 package.[127,128]

2.3. QM/MM Protocol. For the purposes of the present work we extracted five snapshots of the complete system from the classical molecular dynamics to be used in the QM/MM calculations. The first snapshot, which represents a structural configuration that is close to the crystal structure of PSII, is derived from the early equilibration procedure, where we clustered[129] a series of frames from the

https://dx.doi.org/10.1021/jacs.0c08526
J. Am. Chem. Soc. 2020, 142, 18174−18190

trajectory using the CPPTRAJ[130,131] module of AmberTools19. The other four snapshots were derived from the production run, that is, from an unbiasedly evolved, completely hydrated, and thoroughly equilibrated system. These four snapshots are equally spaced from each other, i.e., captured with an interval of 4.0 ns, which ensures that these snapshots are structurally uncorrelated. Inspection of the overall protein structure overlay (Figure S1 of the Supporting Information, SI) of these snapshots confirms that the structural configuration of the protein in these snapshots is distinct. For the QM/MM setup we considered the entire PSII monomer and a total of 8000 water molecules, which includes all the waters presents in the protein cavity, various channels, and ∼7 Å bulk-region around the protein. In order to keep the system neutral, we maintained the required amount of Na^+ ions at their equilibrated positions. The final QM/MM system contains a total of 76 056 atoms.

The QM/MM calculations were performed with ChemShell 3.7,[132−134] where the in-built DL-POLY[135] was used for MM computations, whereas ORCA[103] was the QM engine. Our calculations are based on the electrostatic embedding technique. Covalent bonds were cut using the hydrogen link atom approach. The charge-shift method implemented in ChemShell is used to avoid overpolarization of the QM region by the MM region. For a given snapshot, we carried individual QM/MM geometry optimization calculations of Chl_{D1}, Chl_{D2}, $Pheo_{D1}$, and $Pheo_{D2}$, while the P_{D1}/P_{D2} pair is treated as a single QM unit in QM/MM optimizations due to the close proximity of the two chlorophylls. With such a procedure, we retain the symmetry breaking feature of the vinyl moiety in P_{D1}/P_{D2}, which is otherwise poorly represented by the MM force field. Similar concerns were raised by Mennucci and co-workers,[136] who found overstabilization of the acetyl group of Bacteriochlorophyll *a* by the MM force-field. In addition, with this approach both chromophores of the P_{D1}/P_{D2} pair retain their macrocyclic ring curvature, important for the position of the Q-band,[137,138] induced by their spatial proximity. Therefore, the geometry for all the single point calculations on the individual P_{D1} and P_{D2} is derived directly from the pair-optimized geometry.

During all QM/MM geometry optimizations the model is divided into two parts, active and static. The active region is defined by a QM subregion and an active MM region, whereas the static region remains fixed in the optimization procedure and can only influence the active region through the electrostatic effect of the point charges. In our cases where single chromophore is studied, we chose all residues and cofactors which are ca. 13 Å around the QM region (approximately 1300−1600 atoms). A larger active MM region (15 Å) was chosen for the optimization of the special pair (ca. 2650 atoms). For all the geometry optimizations, we employed the PBE functional[139] and Def2-TVZP basis set,[140] along with D3(BJ) dispersion corrections.[141,142] To speed up the calculations of Coulomb integrals we employed the resolution of identity (RI) approximation,[143,144] in combination with Weigend's universal Def2/J auxiliary basis set.[145] We used tight convergence criteria and a higher than default integration grid (grid6 in ORCA nomenclature) for all optimizations.

2.4. Computation of Excitation Energies. The computation of vertical excitation energies (VEE) in this work is performed on the QM/MM optimized geometries of the chromophores. The explicit effect of the entire PSII monomer environment on the electronic properties of chromophores is included through point-charges, handled by the *orca_pc* module which adds the contribution of the charges in the one-electron matrices and nuclear repulsion. We elucidated the effect of specific protein components on the excitation energies by switching off the corresponding point charges. Full Time-Dependent Density Functional Theory (TD-DFT), i.e., without the Tamm−Dancoff approximation, was used to compute the excited state properties using the range-separated ωB97X-D3(BJ)[146−148] functional along with the Def2-TZVP basis set. The choice of functional was guided by its highly successful application in related studies of biological chromophores[149] and its established superior performance for the treatment of charge-transfer states with TD-DFT.[150] The appropriateness of the functional is additionally confirmed in the present work via direct comparisons with coupled cluster theory. The RIJCOSX approximation[151,152] is used to speed up the calculations. In addition, very tight SCF convergence criteria were set along with higher integration grids (grid6 and gridX7 in ORCA nomenclature) in all cases considered in this work. We have computed 20 roots in all cases. We have also performed calculations with the long-range corrected LC-BLYP[153] functional, with the same settings as described above. In addition to individual chromophores we computed the excited states of groups of adjacent RC chromophores. The selection of pairs and trimers is based on proximity and on existing hypotheses about the primary excitation and charge separation.[26,29] Independently optimized geometries of individual chromophores were used to set up the oligomeric assemblies.

Despite using the best available functionals, known problems in the performance of TD-DFT in general and for charge-transfer states in particular,[154−162] indicate that independent validation beyond DFT is necessary to build confidence in the results,[88,163,164] especially when excited state properties of coupled chromophores are considered. Thus, both in order to obtain results that overcome potential limitations of TD-DFT and to further probe the nature of the excited states of the chromophores with an orthogonal methodology, we employed, for the first time in such a large-scale simulation, the domain based local pair natural orbital (DLPNO) implementation of the similarity transformed equation of motion coupled cluster theory with single and double excitations, STEOM-CCSD.[164−170] A recent study showed this method to provide a highly accurate description of all features of the gas-phase absorption spectrum of chlorophyll *a*,[171] while another study[172] showed that it performs exceptionally well for charge-transfer states, on par with coupled cluster methods that include triple excitations, in contrast to more approximate approaches such as CC2. For the coupled cluster QM/MM calculations, the first of their kind to be conducted on a photosynthetic reaction center, we computed in total 6 roots for each chromophore using the Def2-TZVP(-f) basis set for all atoms. When applied to pairs of chromophores, to maintain feasibility of the coupled cluster calculations the chlorophyll and pheophytin models were truncated by omitting macrocyclic ring substituents. With this procedure, we keep the number of basis functions within the bounds of computational feasibility while maintaining the chemical information regarding the nature and energetic order of excited states in RC chromophore pairs. For the DLPNO-STEOM-CCSD calculations of chromophore assemblies we have resorted to the Def2-SVP basis set and computed 20 roots in total. The RIJCOSX approximation is used to speed up the calculations throughout. "TightPNO" settings were applied for the DLPNO calculations. The $T_{CutPNOsingles}$ cutoff was set to 6.6×10^{-10} and the active space selection keywords "Othresh" and "Vthresh" were set to 5.0×10^{-3}.

3. RESULTS AND DISCUSSION

3.1. Structural Aspects of Pigment−Protein Interactions. The intrinsic photophysical properties of the chromophores are engineered in the protein matrix for efficient light harvesting. In Photosystem II various domains of multichromophoric systems exist, such as internal antenna systems (CP43 and CP47) and the reaction center. The chromophores in the RC, i.e., four chlorophyll *a* and two pheophytin *a* molecules, are symmetrically placed along the D1 (344 residues) and D2 (342 residues) polypeptide chains. These chromophores are situated deep inside the transmembrane region of PSII, and far away from the solvent exposed stromal and lumenal regions. Due to differences in the amino acid sequence of D1 and D2,[14] and overall PSII structural organization, the chromophores may experience distinct strain and electrostatic effects.

The chlorophylls of the P_{D1}/P_{D2} pair are weakly stacked in the middle of the PSII monomer and both of them are axially ligated with histidine residues, His198 for P_{D1} and His197 for

https://dx.doi.org/10.1021/jacs.0c08526
J. Am. Chem. Soc. 2020, 142, 18174−18190

P_{D2} (Figure 3). The accessory chlorophylls Chl_{D1} and Chl_{D2} are axially ligated with a single water molecule, while another

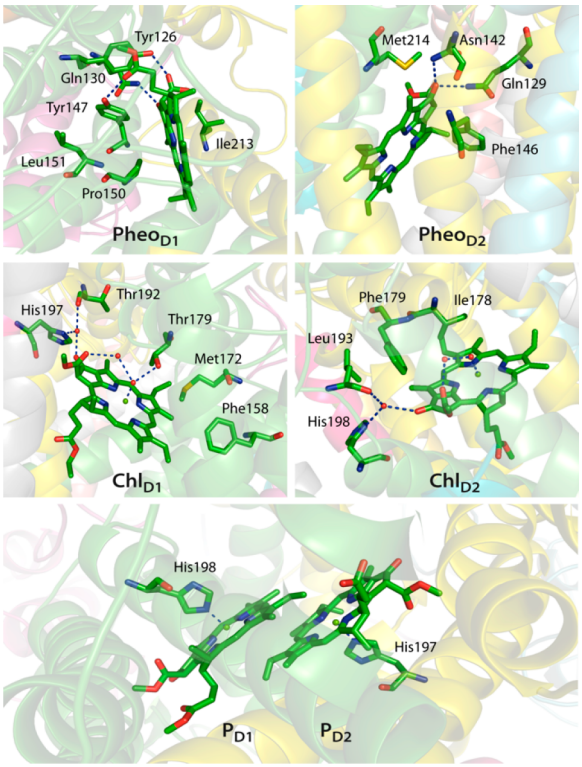

Figure 3. Protein environment around chromophores associated with the reaction center in Photosystem II. Hydrogen bonding interactions are indicated with dashed lines.

water molecule is present in the PSII crystal structure that hydrogen-bonds simultaneously with the axially ligated water and the C-13^2–$COOCH_3$ substituent. However, important differences are found in the second coordination sphere of Chl_{D1} and Chl_{D2}. The axially ligated water forms further hydrogen bond with Thr179 in case of Chl_{D1}, but the axial water of Chl_{D2} does not participate in any further hydrogen bonding and a hydrophobic Ile178 is found instead in its vicinity. Other important structural differences exist in the peripheral region, where the C-13^1 keto group of the macrocyclic ring is hydrogen bonded with a single water molecule. This water molecule is also found to be highly conserved across many high-resolution crystal structures. Interestingly, a recent experimental study using absorption spectroscopy and Resonance Raman techniques by Robert and co-workers[173] showed that hydrogen bonds to the keto group of Chl *a* can fine-tune the absorption properties of the LHCII (Light Harvesting Complex) antenna system. Another investigation by Collini and co-workers[174] showed how such water-mediated interaction with the peripheral substituents can influence the overall conjugation in Chl *a*/*b* found in the water-soluble chlorophyll protein (WSCP). A small number of differences also exist in the immediate environment of the $Pheo_{D1}$ and $Pheo_{D2}$. The C-13^1 keto group of $Pheo_{D1}$ is hydrogen bonded to the Gln130, whereas, the C-13^1 keto group of $Pheo_{D2}$ can establish two hydrogen bonds simultaneously with Gln129 and Asn142. The C-13^2–$COOCH_3$ and C-17^3–COOR groups of $Pheo_{D1}$ hydrogen-bonds to two tyrosines, Tyr147 and Tyr126. However, C-13^2–$COOCH_3$ and C-17^3–COOR groups of $Pheo_{D2}$ are surrounded by hydrophobic residues (Phe255, Phe125, and Phe146).

Analysis of our molecular dynamics trajectories indicates that the D1 and D2 chains are extremely stable throughout the simulations compared to the dynamic evolution of the complete system (Figure 4). This strongly suggests that the

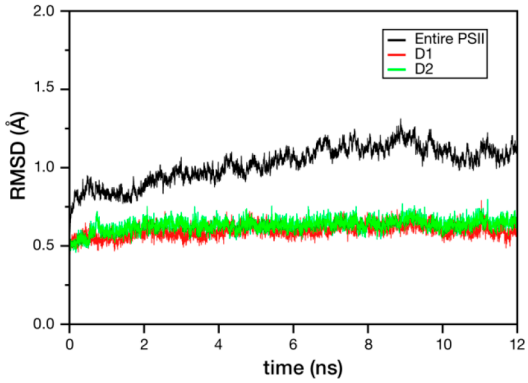

Figure 4. Time evolution of the root-mean-square deviation (RMSD in Å) of the C_α atoms of the complete PSII complex and of the D1 and D2 core polypeptides during the production MD run. Disordered regions of the protein are not considered in the RMSD calculations.

D1 and D2 proteins do not undergo any large-scale conformational change in the PSII core complexes within the time scale of the simulation. The stability of the D1 and D2 poly peptides ensures that the relative orientations of the chromophores stay essentially intact. In terms of individual chromophores (Figures 5 and S2–S7), we observe that the distance between P_{D1} and P_{D2} spans only a very narrow range around the average of ca. 3.5 Å along the simulation. Contrasting behavior is seen between Chl_{D1} and Chl_{D2} with respect to the hydrogen-bonding interactions of their C-13^1 keto groups with the nearby water molecule. This hydrogen bond appears quite constrained in the case of Chl_{D1} but samples a wider range of distances in the case of Chl_{D2}. Finally, we observe that the protein environment around $Pheo_{D2}$ is highly dynamic, with significant degree of rotations for the side-chains of Gln129 and Asn142. In contrast, the hydrogen bonding interaction of $Pheo_{D1}$ with Gln130 remains stable throughout the MD simulation and no large fluctuations in side-chain conformations are observed. Overall, production MD simulations over 12 ns strongly indicate that the environment of the D1 branch chromophores is more rigid and under tighter steric control of the protein matrix than the D2 branch.

3.2. Excitation Profiles of Individual Chromophores.

The protein environment is known to influence the excited state properties of the chromophores in various ways, such as geometric strain, hydrogen bonding, and electrostatic effects. To understand the influence of these factors in a bottom-up fashion, first we computed the excited state properties of individual chromophores using their QM/MM optimized geometries but in the absence of any representation of the protein environment. These gas-phase TD-DFT calculations with the ωB97X-D3(BJ) functional lead to approximately the same $S_0 \rightarrow S_1$ (Q_y) vertical excitation energies for all chromophores, within the narrow range of 1.920–1.943 eV (see Figure 6 and Tables S1–S4). Similar results were

https://dx.doi.org/10.1021/jacs.0c08526
J. Am. Chem. Soc. 2020, 142, 18174–18190

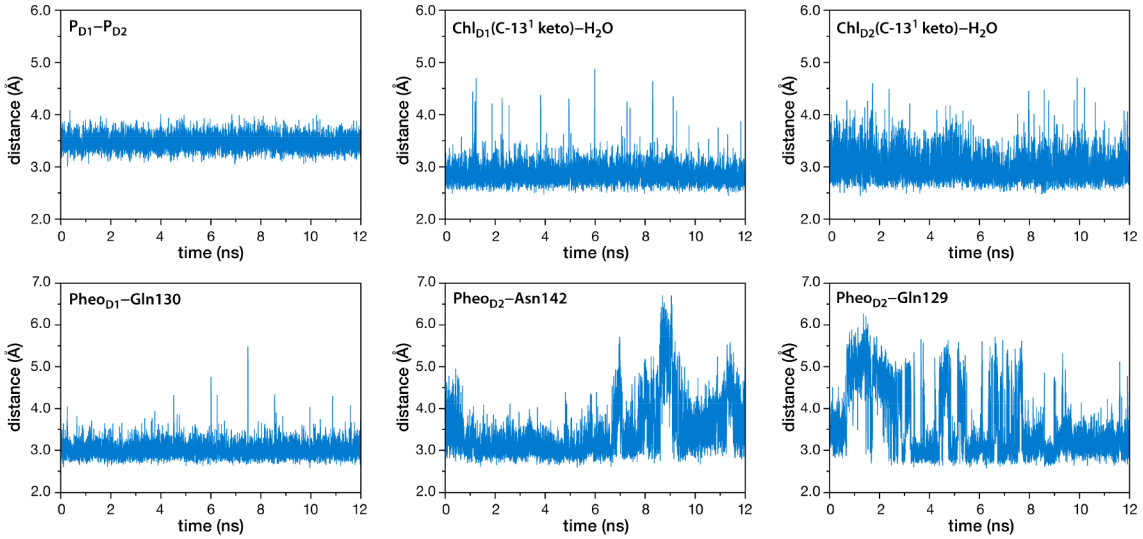

Figure 5. Time evolution of selected distances involving RC chromophores during the production MD run. Further details are provided in the SI.

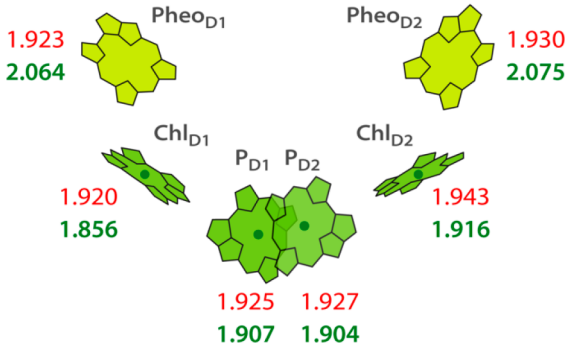

Figure 6. Lowest-energy excitations (site energies), in eV, of PSII reaction center chromophores without (red) and with (green) the protein electrostatic environment. The calculations were performed with the ωB97X-D3(BJ) functional using QM/MM geometries.

obtained in past studies[62,65] where a uniform dielectric medium was used to mimic the protein environment. As the geometries of the pigments already incorporate the structural effects of the protein matrix, we conclude that the protein-induced strain on the macrocyclic rings is *not* responsible for inducing functional asymmetry in the localization of the lowest excited state in the RC.

Subsequently, excited state calculations using the same QM/MM optimized geometries were performed in a TD-DFT–QM/MM fashion, i.e., in the presence of the protein electrostatic environment (values in green in Figure 6). Two striking observations can be made: (a) all four chlorophyll *a* chromophores of the RC are red-shifted upon embedding in the protein environment, whereas both pheophytins are blue-shifted (~0.1 eV), and (b) Chl_{D1} is the most strongly red-shifted pigment. Interestingly, the "special pair" P_{D1}–P_{D2} displays negligible internal asymmetry in terms of site energies either with or without the protein matrix. The identification of Chl_{D1} as the pigment with the lowest energy excited state supports previous interpretations that account for the effects of the protein matrix.[21−23,67,76,175]

Different quantum chemical methods agree on the absence of noticeable asymmetry in calculations that omit the electrostatic effect of the protein, even though they provide different absolute values for the excitations, which is anticipated (see SI). What is important for the fundamental question of the emergence of excitation asymmetry is the reliable reproduction of the nature and extent of red or blue shift of the lowest excitation when the electrostatic effect of the protein matrix is included in the calculations. Comparison of the shifts produced by different methods (Table 1) shows that

Table 1. Comparison of Electrochromic Shifts (in eV) of Site Energies (Q_y) from the Gas-Phase to the Protein Matrix for Individual Reaction Center Chromophores, Computed with TD-DFT Using Two Different Range-Separated Density Functionals and with DLPNO-STEOM-CCSD

	ωB97X-D3(BJ)	LC-BLYP	DLPNO-STEOM-CCSD
P_{D1}	−0.018	−0.016	−0.020
P_{D2}	−0.023	−0.021	−0.015
Chl_{D1}	−0.064	−0.062	−0.067
Chl_{D2}	−0.027	−0.025	−0.025
$Pheo_{D1}$	+0.141	+0.136	+0.142
$Pheo_{D2}$	+0.145	+0.140	+0.177

ωB97X-D3(BJ) and LC-BLYP produce very similar shifts, in line with those of DLPNO-STEOM-CCSD calculations. The coupled cluster results agree best with ωB97X-D3(BJ). The only significant difference between the two methods is that STEOM-CCSD predicts an even stronger blue shift for $Pheo_{D2}$.

It is evident that two types of protein matrix electrostatic asymmetry develop within the transmembrane region: (a) *transverse asymmetry*, which red-shifts the chlorophylls and blue-shifts the pheophytins, and (b) *lateral asymmetry*, which differentiates the D1 and D2 branches. This is also reflected in the electrostatic potential as experienced by the chromophores in the protein matrix. The potential is indeed distinct along D1 and D2, and the pheophytins reside in a relatively more positive electrostatic potential pocket (Figure 7). Therefore, the intrinsic protein electrostatic environment is the principal factor in modulating the distribution of excitation energies of RC chromophores and giving rise to both chlorophyll–pheophytin asymmetry (transversely) and D1–D2 branch asymmetry (laterally).

https://dx.doi.org/10.1021/jacs.0c08526
J. Am. Chem. Soc. 2020, 142, 18174−18190

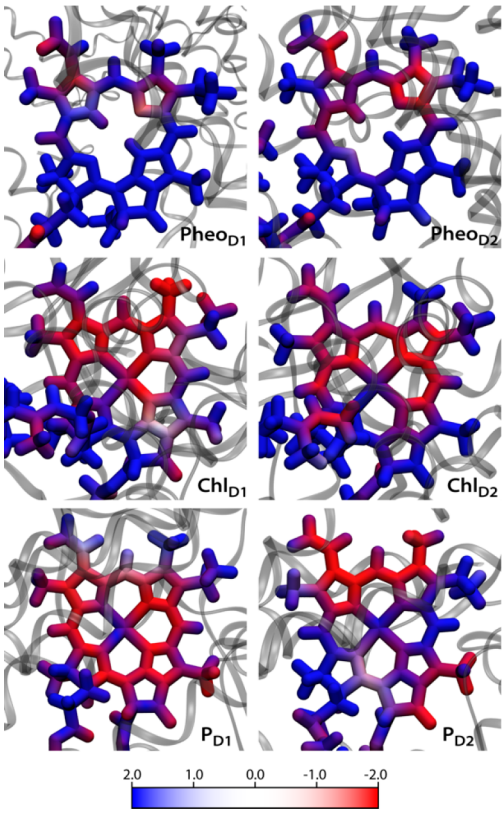

Figure 7. Electrostatic potential experienced by the reaction center chromophores (in kT/e) inside the protein matrix. The calculations were performed using the APBS (Adaptive Poisson−Boltzmann Solver) program[176] on the crystal-structure-like configuration of the protein (snapshot 1).

The asymmetry induced by protein electrostatics can be associated with differences between the D1 and D2 sequences, spatial proximity of charged residues and redox active cofactors, and the overall organization of extrinsic proteins, which differ in cyanobacteria, algae, and higher plants. Each chromophore experiences the intrinsic protein electrostatics differently because of their location and orientation with respect to the transmembrane region. Therefore, the asymmetry in the reaction center is not an intrinsic property related to the spatial arrangement of the chromophores. This explains why past computational studies that used at most a uniform dielectric to mimic the protein environment[62,65] reported essentially the same Q_y energies for the individual RC chromophores but did not reproduce the excitation asymmetry that is a feature of the real system. It is noted that previous works[20,23,33] employing spectral modeling have assigned nearly equal Q_y energies of chlorophylls and pheophytins. This is not in line with the present results and further work is required for a confident analysis of the optical spectrum. It cannot be excluded that a more elaborate theoretical treatment of the protein environment, for example with inclusion of polarization effects, may provide a better balance between the spectral fitting and the quantum chemical results.

Identification of the key protein components that give rise to asymmetry in the reaction center is important for our overall understanding of unidirectional electron transfer. Protein electrostatics are responsible for red-shifting Chl$_{D1}$ by 0.064 eV (516 cm^{-1}), which is by far the most drastic protein matrix effect on a single chromophore. The major contributors to this red-shift include Met172 (76 cm^{-1}) and Phe158 (48 cm^{-1}). Interestingly, the pseudosymmetric partners of these Chl$_{D1}$ "red-shifters" are *different* on the Chl$_{D2}$ side, which suggests that localized factors control the asymmetry around these chlorophylls. Additional contributions arise from P$_{D1}$ (79 cm^{-1}), and from the chloride ions in the vicinity of the OEC (61 cm^{-1}). However, major contributors toward the 0.141 eV (1137 cm^{-1}) blue shift of Pheo$_{D1}$ were found to be mostly the closely lying amino acids and cofactors, including Tyr147 (115 cm^{-1}), Pro150 (89 cm^{-1}), Chl$_{D1}$ (66 cm^{-1}), Leu151 (52 cm^{-1}), and Ile213 (28 cm^{-1}).

It has been suggested that the OEC or residues that coordinate the Mn_4CaO_5 cluster contribute to the red shift of Chl$_{D1}$.[67] Our calculations show that this is not the case and we attribute this to incorrect MM setup. Specifically, the use of integer charges for the Mn ions of the OEC in accordance to formal oxidation states results in exaggerated concentration of charge on the inorganic core and individually on its ligands. The physically motivated approach is to use distributed charges as in the present work, deducing them from RESP calculations that treat the Mn_4CaO_5 cluster *and all its covalently bonded ligands* as a single chemical entity. This eliminates long-range Coulombic artifacts. Beyond the fundamental technical aspect, attribution of a major site energy determining role to the OEC is conceptually problematic because normal function of the reaction center is required for photoassembly of the OEC[177−179] and hence must be independent of its presence.

Although we pinpointed certain major contributors to the observed shifts, the total shifts in each case are not completely produced by a limited list of contributions, but instead an ever increasing number of residues and cofactors with ever smaller contributions can be found. Therefore, not only localized but also global electrostatics[23] play a key role to produce the total shift compared to the gas-phase result, which shows that the evolutionary optimization of the enzyme operates on all scales. The present description has a parallel in the photosynthetic bacterial reaction center, where the chromophores were also found to be embedded in a dielectrically asymmetric environment.[180,181]

Some comments on methodological issues must be made at this point. First of all, the above observations underline the necessity of the QM/MM approach for obtaining meaningful results. We confirm that enlarging a gas-phase QM model by including several selected amino acid residues around each chromophore does not even begin to approximate the full QM/MM results. Another critical methodological issue relevant to studies that employ QM or QM/MM methods is the use of experimental (crystallographic) structures for the pigments. This choice is detrimental for quantum chemical approaches (alternative approaches[23,175,182] for studying site energies are largely unaffected) because experimental structures typically do not exhibit correct bond length alternation of conjugated systems,[86,87] often not even qualitatively. This is, however, the key geometric parameter that governs the electronic structure of the ground and excited states because it directly determines the nature and energetics of frontier orbitals. Therefore, the use of experimental geometries introduces a fundamental inconsistency between the quantum chemical approach and the structural model on which it operates, leading to randomization of results through uncontrolled errors. When this is coupled with the neglect of protein matrix electrostatics, the combined methodological deficiencies practically guarantee that the quantum chemical

https://dx.doi.org/10.1021/jacs.0c08526
J. Am. Chem. Soc. 2020, 142, 18174−18190

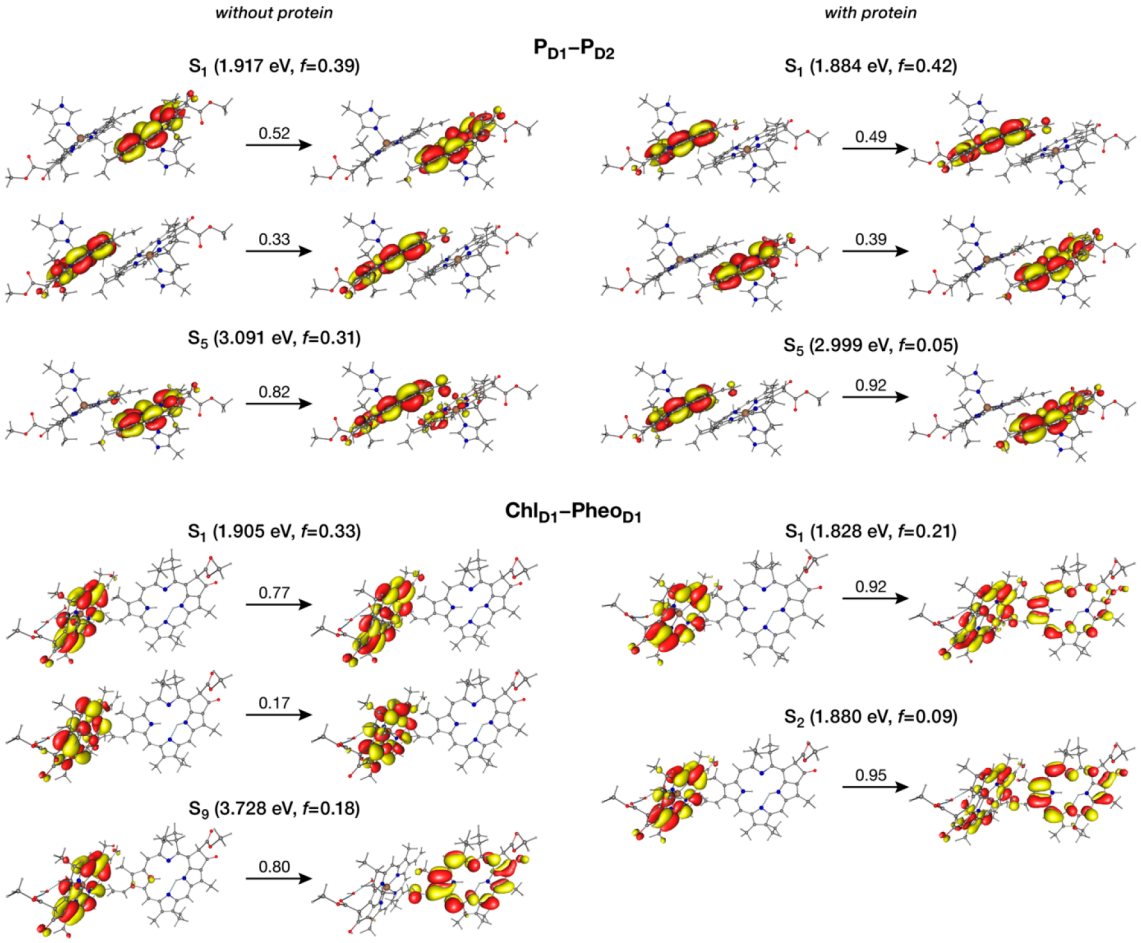

Figure 8. A detailed description of the identity and nature of the lowest excited state (S_1) and of the first root with significant charge transfer character for the P_{D1}–P_{D2} and Chl_{D1}–$Pheo_{D1}$ pairs in terms of Natural Transition Orbitals (NTOs) and relative contributions to a given excitation. In the case of Chl_{D1}–$Pheo_{D1}$ both states depicted have significant CT character. Vertical excitation energies (in eV) and oscillator strengths (f) are provided for each state depicted (from ωB97X-D3(BJ) TD-DFT calculations), comparing the results in the absence (left) and in the presence (right) of the electrostatic effect of the complete PSII monomer.

results are of little relevance to the real system (for example, a study[183] that satisfies none of these conditions finds the lowest-energy excitation of the RC to be localized on the $Pheo_{D1}$). The same holds for the direct use of force-field (MM) geometries.[67] These considerations apply equally to the quantum chemical treatment of multiple RC chromophores, an even more delicate case because of the sensitivity of interpigment charge-transfer states on both the geometries of interacting chromophores and on protein matrix electrostatics.

3.3. Excitation Profiles of Chromophore Pairs. Intermolecular charge-transfer (CT) excitations, i.e., those where the electron donor and acceptor are two different chromophores, are central in the function of reaction centers across photosynthetic organisms.[36,37,39] Although site energies already reveal a lot about the RC of PSII, understanding the initiating events of productive primary photoexcitation requires direct insight into the excitation profiles of multiple chromophores. To obtain this information we have systematically studied the excited states of pairs of chromophores in the D1 and D2 branches, i.e., P_{D1}–P_{D2}, P_{D1}–Chl_{D1}, P_{D2}–Chl_{D2}, Chl_{D1}–$Pheo_{D1}$, and Chl_{D2}-$Pheo_{D2}$.

The "special pair" holds a special status both in bacterial reaction centers[13,184] and in Photosystem II,[13,26,29] therefore we focus on this one first. TD-DFT calculations performed in the gas phase (using the QM/MM optimized geometry of the pair) reveal that the nature of the lowest excitation, at 1.917 eV, is a linear combination of local excitations (LE) on P_{D1} and P_{D2} individually. Analysis of the excitations in terms of natural transition orbitals (NTOs) is provided in Figure 8. The first excitation with CT character (root 5), $P_{D1}^{-}P_{D2}^{+}$, is situated considerably higher in energy, at 3.091 eV. In comparison to the gas-phase results, TD-DFT QM/MM computations performed with full account of protein electrostatics result in an overall red-shift of the lowest excited state, which is now predicted at 1.884 eV, however the nature of the excited state remains the same, i.e., superposition of local excitations. We note that this is what one would expect in a Frenkel excitation picture and that the second excited state (S_2, at 1.911 eV, see also Table S5) is also a linear combination of the two local excited states. Protein electrostatics affect the "directionality" of the lowest charge transfer state ($P_{D1}^{+}P_{D2}^{-}$) but do not stabilize it significantly compared to the gas-phase result (2.999 eV).

Next, we have investigated the symmetry-related P_{D1}-Chl_{D1} and P_{D2}-Chl_{D2} pairs along the active and inactive chains. The lowest excited state (1.905 eV) computed from gas-phase calculations on P_{D1}-Chl_{D1} is a linear combination of local excitations on Chl_{D1} and P_{D1}, whereas the first CT state (root

https://dx.doi.org/10.1021/jacs.0c08526
J. Am. Chem. Soc. 2020, 142, 18174−18190

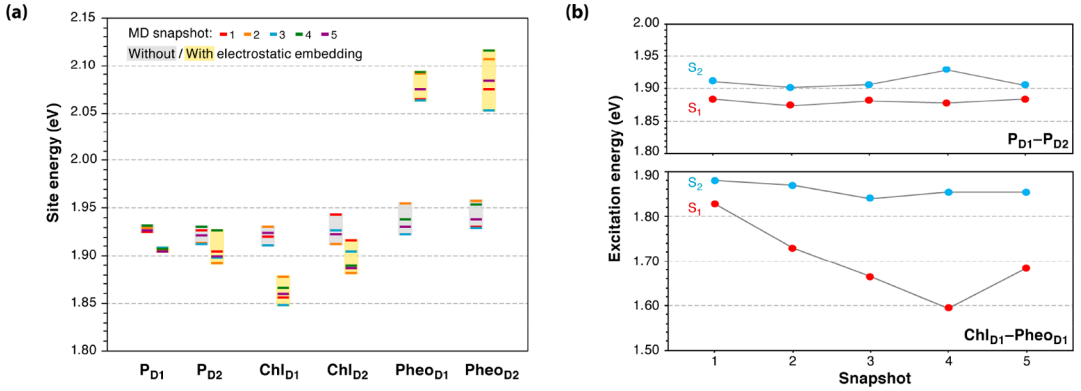

Figure 9. Effect of protein conformational flexibility on the first excited state (in eV) of the individual chromophores (a) and on the two lowest excited states of the P_{D1}−P_{D2} and Chl_{D1}−$Pheo_{D1}$ pairs of chromophores (b) from ωB97X-D3(BJ) TD-DFT QM/MM calculations on QM/MM geometries optimized individually for each snapshot. Snapshot 1 represents the "crystal-like-conformation" of the protein, whereas snapshots 2−5 were derived from the production molecular dynamics simulations with regular intervals of 4 ns.

9, P_{D1}^{-} Chl_{D1}^{+}) was found much higher in energy (3.639 eV). Protein electrostatics induce an overall red shift in the lowest excited state (1.843 eV) and character alteration of the lowest excited state, which becomes a local excitation on Chl_{D1}. In addition, the lowest CT state (root 5) changes in directionality (P_{D1}^{+} Chl_{D1}^{-}) and is found much lower in energy, at 3.130 eV. Similar observations are made for the P_{D2}−Chl_{D2} pair, where in relation to the gas-phase results the protein electrostatics induces a red-shift of the lowest excited state (1.895 eV, LE on P_{D2}), lowers the energy and alters the directionality of the first CT state (P_{D2}^{+} Chl_{D2}^{-}, root 5, 3.232 eV, see also Table S7).

In the case of the Chl_{D2}-$Pheo_{D2}$ pair (see Figure S8), the gas-phase calculations indicate that the lowest energy state (1.926 eV) is a local excitation on Chl_{D2}, whereas the lowest CT state ($Chl_{D2}^{+}Pheo_{D2}^{-}$, root 9) is located at 3.726 eV. Within the protein matrix we computed a slight red-shift of the lowest excited state (1.903 eV, LE on Chl_{D2}) and a significant stabilization of the CT state ($Chl_{D2}^{+}Pheo_{D2}^{-}$, root 3) at 2.092 eV.

The most profound demonstration of protein matrix control is observed in the case of the Chl_{D1}−$Pheo_{D1}$ pair. The nature of the lowest excited state at 1.905 eV obtained from the gas-phase calculations on the Chl_{D1}−$Pheo_{D1}$ is primarily a local excitation on the Chl_{D1}. The first CT state (root 9, $Chl_{D1}^{+}Pheo_{D1}^{-}$) is much higher in energy (3.728 eV). In this case, however, protein electrostatics drastically reorganize the excitation profile of the pair. The lowest excited state is computed at 1.828 eV and has significant $Chl_{D1}^{+}Pheo_{D1}^{-}$ charge transfer character (Figure 8). Crucially, this particular CT state marks the lowest-energy excited state among all chromophore pairs of the PSII RC. In fact, not only the first but also the second excited state computed for this pair display significant or dominant CT character favoring excitation from Chl_{D1} to $Pheo_{D1}$. The picture obtained from the NTOs is consistent with the difference densities computed for these roots, as will also be shown for the additional MD snapshots discussed in the present work and which have pure $Chl_{D1}^{+}Pheo_{D1}^{-}$ charge-transfer character (vide infra).

The above results are in line with observations from Stark spectroscopy,[36,37] where the $Chl_{D1}^{+}Pheo_{D1}^{-}$ CT state was found to be mixed with LE on Chl_{D1}. This mixing was proposed to be crucial for initiating charge separation in the RC. A similar observation was made by Valkunas and co-workers,[66] where a good fit of the Stark spectrum (using complex time-dependent Redfield theory) was obtained with inclusion of the $Chl_{D1}^{+}Pheo_{D1}^{-}$ CT state, which was found to be more important in reproducing the Stark spectrum than the CT state originating from $P_{D1}^{-}P_{D2}^{+}$.

Calculation of the excited states of the Chl_{D1}−$Pheo_{D1}$ pair using the conductor-like polarizable continuum model (CPCM)[185,186] with a constant dielectric (ε = 4, appropriate for the transmembrane region) does not produce significant differences in the excitation spectrum of the chromophore pair compared to the gas-phase results. The lowest gas-phase CT state (S_9, 3.728 eV) is only marginally stabilized by CPCM (S_8, 3.592 eV). Overall the nature of all excited states remains essentially indistinguishable from the gas-phase TD-DFT spectrum, and hence the continuum dielectric approach is no substitute for the electrostatically asymmetric protein matrix.

Even by using one of the best available DFT methods, the fact that we predict the lowest excited state to have dominant CT character creates the need for further confirmation, because the correct prediction of CT character has been historically a challenge for TD-DFT. The only definitive way to achieve this is to go beyond DFT. Excited states of truncated pigment pairs computed by DLPNO-STEOM-CCSD (see discussion in the SI and Tables S15 and S16) confirm the nature of excited states obtained with ωB97X-D3(BJ), and therefore fully support the above conclusions beyond any conceivable uncertainty arising from the level of theory.

In conclusion, our QM/MM results on monomer and pair excitation energies confirm Chl_{D1} as the pigment with the lowest site energy and furthermore identify the lowest excitation of the RC as associated with a CT state of the Chl_{D1}−$Pheo_{D1}$ pair.

3.4. Excited States of the P_{D1}−P_{D2}−Chl_{D1} Trimer. The results presented above firmly support a CT excited state of the type $Chl_{D1}^{+}Pheo_{D1}^{-}$ as the lowest energy excited state among pairs of RC chromophores, and hence suggest that actual charge separation would occur accordingly within this pair. An alternative pathway mentioned in the introduction as one of the possibilities under discussion involves excitation of P_{D1} or the P_{D1}−P_{D2} pair with charge transfer to Chl_{D1}. To investigate this possibility we conducted the same type of QM/MM calculations with simultaneous inclusion of all three relevant chromophores in the QM region (P_{D1}, P_{D2}, and Chl_{D1}). The TD-DFT QM/MM results presented and analyzed in terms of NTO compositions in Table S17 show that the lowest excited

https://dx.doi.org/10.1021/jacs.0c08526
J. Am. Chem. Soc. 2020, 142, 18174−18190

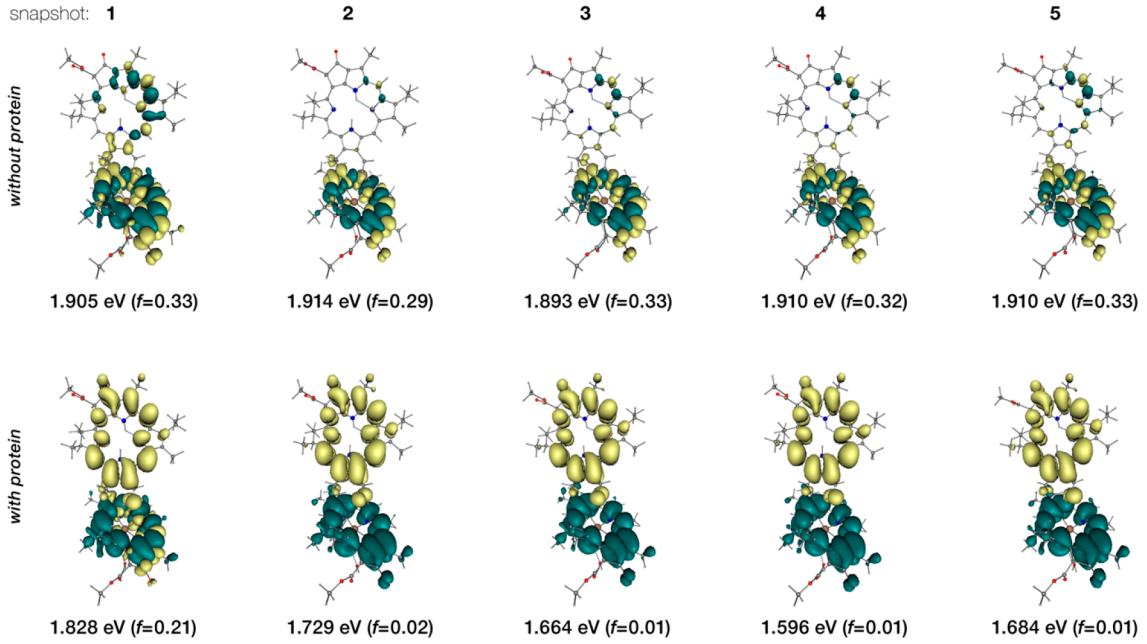

Figure 10. Difference densities describing the lowest excitation of the Chl_{D1}−$Pheo_{D1}$ pair with exclusion (top row) and inclusion (bottom row) of protein electrostatics. With explicit consideration of the protein matrix the lowest excited state of the RC has dominant $Chl_{D1}^{+}Pheo_{D1}^{-}$ charge transfer character in the "crystal-like-conformation" of snapshot 1 and exclusive charge transfer character in the production MD snapshots 2−5.

state of the trimer (S_1 at 1.836 eV) is fully localized on Chl_{D1}, which is consistent with the attribution of the lowest site energy of the RC to this pigment. The second and third (S_2 at 1.880 eV and S_3 at 1.910 eV) are localized excitations on P_{D1} and P_{D2}. Charge transfer states begin to appear above 3 eV. The lowest is a CT state within the P_{D1}−P_{D2} pair ($P_{D1}^{+}P_{D2}^{-}$, S_7 at 3.050 eV), while the first CT state with $P_{D1}^{+}Chl_{D1}^{-}$ CT character is S_8 at 3.093 eV. These results are in line with those obtained for monomers and dimers. Therefore, the present data on the trimer exclude the possibility of an energetically accessible CT excited state within the RC that involves delocalization of negative charge onto Chl_{D1}, and strongly disfavor the hypothetical participation of an anionic Chl_{D1} species in native PSII charge separation.

3.5. Dynamic Control of Low-Energy Charge-Transfer States. In view of the key role of the electrostatic environment described above, it is interesting to investigate if the dynamic evolution of the protein conformation influences the excited state properties of the RC established so far within a single structural configuration of PSII. For this purpose, we performed the same set of excited state calculations, each with individually optimized QM/MM geometries, on structurally independent snapshots obtained from the molecular dynamics simulations. These snapshots were obtained from unbiased production simulations of the PSII−membrane complex, i.e., with no restraints or constraints. We chose four distinct structural configurations of the PSII−membrane complex with a consecutive interval of 4 ns. This has the advantage that the excited state properties are computed on uncorrelated protein configurations that are removed from the crystal structure minima and are properly hydrated and equilibrated with the surrounding environment.

The overall trend in the respective blue and red-shift of the individual RC chromophores and the relative ranking of the Q_y excitation energies remains the same, i.e., Chl_{D1} has the lowest site energy (Figure 9). Focusing on chromophore pairs, we find that the lowest-lying excited state of the RC remains on the Chl_{D1}−$Pheo_{D1}$ pair and retains its CT character ($Chl_{D1}^{+}Pheo_{D1}^{-}$) irrespective of the dynamics of the protein. The above observations suggest that the nature of the intrinsic electric field of the protein matrix, and the resulting excitation asymmetry are essentially unperturbed by the conformational dynamics of the protein. Figure 10 depicts difference densities for the lowest excitation of the Chl_{D1}−$Pheo_{D1}$ pair, which also demonstrate that the effect of the protein matrix is the same both in the crystallographic conformation of the protein and in the selected MD snapshots. Overall, we conclude that asymmetry does not arise as a result of the random conformational fluctuations. However, our findings indicate that the conformational flexibility of the PSII complex plays another important role.

Protein dynamics are seen to affect chromophore pairs in different ways. The conformational flexibility of the protein has little impact on the excited state properties of the inactive branch or of the P_{D1}−P_{D2} pair (Figures 9 and S9), whereas there is a significant impact on the Chl_{D1}−$Pheo_{D1}$ pair of the active branch, where we observe high sensitivity in the energy of the first excited state. For the conformations of the protein studied here, we find the S_1 states with dominant (snapshot 1) to pure (all snapshots along the MD) $Chl_{D1}^{+}Pheo_{D1}^{-}$ CT character in the range 1.828 eV (678 nm) to 1.595 (777 nm). Although the absolute computed values are not suggested to be "exact", since there is a dependence of the absolute values on the choice of QM method, it is interesting to note that this is beyond the nominal threshold for oxygenic photosynthesis of 680 nm (1.82 eV).

We stress that the number of snapshots used here is very small and a considerably more extensive sampling of the MD trajectory would be needed for quantitative analysis. Nevertheless, the present observations serve adequately as demonstration of principle, namely that the intrinsic electrostatic environment and flexibility of the protein are responsible for enabling access to low-energy charge-transfer states. This implies that protein matrix dynamics can push the red limit of

https://dx.doi.org/10.1021/jacs.0c08526
J. Am. Chem. Soc. 2020, 142, 18174−18190

oxygenic photosynthesis even in species that do not benefit from alternative types of chlorophyll (*d* or *f*). In this sense, specific variants of core PSII proteins available to different organisms might be utilized to adjust the red limit in response to environmental conditions not only by presenting alternate localized electrostatic contributors to critical pigments but also by favoring different distribution of global protein conformations. Therefore, electrostatic control by the dynamically evolving protein matrix must be considered equally important to the intrinsic absorption properties of participating chromophores in determining the red limit of photosynthesis.

3.6. Implications for Charge Separation Pathways. The computational results presented above form a solid basis for exploring the physiological function of the reaction center in PSII and connecting with various experimental observations. Studies on sunflower and bean leaves,[43] spinach,[38] green algae,[46] and cyanobacteria[47] showed that the known threshold for charge-separation in oxygenic photosynthesis can be pushed to the far-red region.[38,40,45] Pettai et al.[43,44] reported that higher plants can evolve oxygen using wavelengths as long as 780 nm. Hughes et al.[45] showed that charge separation in PSII can be induced with light of 690−730 nm wavelength (1.7−1.8 eV) at 1.7 K. Similarly, Styring and co-workers[38,40] documented generation of the cation radical in RC using far-red light (up to 750 nm), however a decrease in the overall charge-separated centers was observed with increasing wavelength. Furthermore, it was suggested that a significant population of the Chl_{D1} cation radical is trapped at cryogenic conditions (5 K) and that Tyr161 (Y_Z) is the preferred electron donor in this case over the Cyt-b_{559}/Chl_Z/Car_{D2} pathway (see Figure 1) in far-red light at 5 K. This is fully consistent with our results, which show the "dark" low-lying CT states of the Chl_{D1}−$Pheo_{D1}$ pair to be in the red and far-red region. This implies that after charge separation within this pair takes place, the cation radical would initially be formed on Chl_{D1}. The hole would subsequently migrate to P_{D1} under physiological conditions. Our results are also in very good agreement with the suggestion that Y_Z becomes the preferred electron donor under far-red light at 5 K. The migration of the Chl_{D1} hole to the special pair would require a reorganization of the protein environment that is probably inhibited at cryogenic temperature, resulting in Y_Z becoming an electron donor to Chl_{D1}. Further EPR experiments[39] showed that charge separation upon light excitation is wavelength-dependent, leading to the hypothesis that P_{D1} is excited with visible light (532 nm), whereas Chl_{D1} is excited with far-red light.[39] Our results on the P_{D1}−P_{D2}−Chl_{D1} trimer do not support the presence of any energetically accessible CT state that could lead directly to productive charge separation along the D1 branch, but the conditions under which the special pair may function as the primary donor will need further studies to be clarified.

The present results are also of relevance to understanding RC function in organisms that employ alternative types of chlorophyll. Specifically, some cyanobacteria acclimatized to far-red light synthesize Chl *d* (*Acaryochloris marina*)[187] or Chl *f* (*Chroococcidiopsis thermalis*)[49,188] (absorption maxima at 710 and 750 nm, respectively) with alterations of chlorophyll pigments in the light harvesting antennae and possibly in the reaction centers themselves. The existence and location of Chl *d* pigments in the RC is a subject of debate.[189,190] In the case of *C. thermalis* Nürnberg et al.[49] assigned Chl *f* to be the Chl_{D1} position, while recent work by Judd et al.[191] demonstrated the likelihood of P_{D2} being occupied by Chl *f*. Future work will evaluate these possibilities using the QM/MM approach presented in this study.

Finally, our results indicate that protein conformational flexibility would play a critical role in charge separation and subsequent oxygen evolution with far-red light. Due to the high dependence of the far-red absorption capability of Chl_{D1}−$Pheo_{D1}$ on conformational dynamics, only a fraction of PSII centers[38] could lead to formation of the charge-separated state in far-red. Since four "productive" charge separation events are required to make one O_2 molecule, there is reduced likelihood that the OEC can advance regularly under these conditions, i.e., that subsequent far-red charge separations can occur on-time to advance the catalytic cycle outcompeting recombination. The fact that low O_2 evolution is observed in cyanobacterial and higher-plant PSII excited with far-red light[43,49] is consistent with this scenario.

4. CONCLUSIONS

We presented large scale MM−MD and QM/MM results on a complete membrane embedded PSII monomer, focusing on excitation energies of single and paired reaction center chromophores. The quantum mechanical level of theory in the QM/MM calculation of excitation energies include long-range corrected TD-DFT and the DLPNO implementation of the similarity transformed equation of motion coupled cluster theory with single and double excitations, STEOM-CCSD. The approach presented here serves as a reference for future studies of the reaction center. Any deviations of past reports from the results of the present work for either single or multiple chromophores can be directly traced to neglect of one or more of the methodological pillars defined in the present study.

Our results demonstrate explicitly that the excitation asymmetry in the reaction center of PSII is not an intrinsic property of RC chromophores and does not originate from their distinct geometric distortion or coordination. Asymmetry is not observed, and cannot be understood, in the absence of the protein environment. It arises exclusively through the electrostatic effect of the protein matrix. We demonstrated that the electrostatic field of the protein acts by shifting the intrinsic site energies of the chlorophylls and pheophytins in opposite directions. Red-shifting of chlorophylls versus blue-shifting of pheophytins creates transverse asymmetry with respect to the membrane normal. Preferential lowering of site energies and most importantly of charge-transfer excited states along the D1 side of the Photosystem II creates lateral asymmetry. In the presence of the protein matrix the pigment with the lowest site energy is Chl_{D1} and the lowest excited state within the reaction center is a state of charge transfer character localized at the Chl_{D1}−$Pheo_{D1}$ pair. Therefore, the present results support assigning this pair as the site of initial charge separation in PSII. The central P_{D1}−P_{D2} chlorophylls do not present low-energy charge transfer excitations internally, while the possibility of charge transfer excitation from this pair to Chl_{D1} is excluded. Finally, protein dynamics have only weak influence on the localization of low-energy excitations, but enable charge transfer excitations within the Chl_{D1}−$Pheo_{D1}$ pair to occur with far-red light.

https://dx.doi.org/10.1021/jacs.0c08526
J. Am. Chem. Soc. 2020, 142, 18174−18190

■ ASSOCIATED CONTENT

Supporting Information

The Supporting Information is available free of charge at https://pubs.acs.org/doi/10.1021/jacs.0c08526.

Figures S1−S11 and Tables S1−S20, overview of site energies of the PSII RC chromophores; excited state properties of interacting pigment pairs with ωB97X-D3(BJ); excited state properties of interacting pigment pairs with LC-BLYP; comparison of TDDFT and DLPNO-STEOM-CCSD; excited states of the P_{D1}−P_{D2}−Chl_{D1} trimer; low-lying excited states of interacting chromophores from additional protein configurations; D1 and D2 sequence alignment from different photosynthetic organisms; Cartesian coordinates of optimized chromophores; and additional references (PDF)

■ AUTHOR INFORMATION

Corresponding Author

Dimitrios A. Pantazis − *Max-Planck-Institut für Kohlenforschung, 45470 Mülheim an der Ruhr, Germany;* orcid.org/0000-0002-2146-9065; Email: dimitrios.pantazis@kofo.mpg.de

Authors

Abhishek Sirohiwal − *Max-Planck-Institut für Kohlenforschung, 45470 Mülheim an der Ruhr, Germany; Fakultät für Chemie und Biochemie, Ruhr-Universität Bochum, 44780 Bochum, Germany;* orcid.org/0000-0002-4073-7627

Frank Neese − *Max-Planck-Institut für Kohlenforschung, 45470 Mülheim an der Ruhr, Germany;* orcid.org/0000-0003-4691-0547

Complete contact information is available at: https://pubs.acs.org/10.1021/jacs.0c08526

Notes

The authors declare no competing financial interest.

■ ACKNOWLEDGMENTS

The authors gratefully acknowledge support by the Max Planck Society. We thank Dr. Ragnar Björnsson for his valuable assistance with the QM/MM computations. The authors thank the Max Planck Computing and Data Facility (Garching) for computational resources. This work was funded by the Deutsche Forschungsgemeinschaft (DFG, German Research Foundation) under Germany's Excellence Strategy—EXC 2033−390677874−RESOLV.

■ REFERENCES

(1) Blankenship, R. E. *Molecular Mechanisms of Photosynthesis*; 2nd ed.; Wiley: Chichester, 2014; p 312.

(2) *Photosystem II. The Light-Driven Water:Plastoquinone Oxidoreductase*; Wydrzynski, T., Satoh, K., Eds.; Springer: Dordrecht, 2005; Vol. 22.

(3) Shevela, D.; Björn, L. O.; *Govindjee Photosynthesis: Solar Energy for Life*; World Scientific: Singapore, 2017; p 204.

(4) Ferreira, K. N.; Iverson, T. M.; Maghlaoui, K.; Barber, J.; Iwata, S. Architecture of the Photosynthetic Oxygen-Evolving Center. *Science* **2004**, *303*, 1831−1838.

(5) Umena, Y.; Kawakami, K.; Shen, J.-R.; Kamiya, N. Crystal structure of oxygen-evolving photosystem II at a resolution of 1.9 Å. *Nature* **2011**, *473*, 55−60.

(6) Barber, J. Photosystem II: the water splitting enzyme of photosynthesis and the origin of oxygen in our atmosphere. *Q. Rev. Biophys.* **2016**, *49*, e14.

(7) Krewald, V.; Retegan, M.; Pantazis, D. A. Principles of Natural Photosynthesis. *Top. Curr. Chem.* **2015**, *371*, 23−48.

(8) Dekker, J. P.; Van Grondelle, R. Primary charge separation in Photosystem II. *Photosynth. Res.* **2000**, *63*, 195−208.

(9) Holzwarth, A. R.; Müller, M. G.; Reus, M.; Nowaczyk, M.; Sander, J.; Rögner, M. Kinetics and mechanism of electron transfer in intact photosystem II and in the isolated reaction center: Pheophytin is the primary electron acceptor. *Proc. Natl. Acad. Sci. U. S. A.* **2006**, *103*, 6895−6900.

(10) Rutherford, A. W.; Osyczka, A.; Rappaport, F. Back-Reactions, Short-Circuits, Leaks and Other Energy Wasteful Reactions in Biological Electron Transfer: Redox Tuning to Survive Life in O_2. *FEBS Lett.* **2012**, *586*, 603−616.

(11) Raszewski, G.; Renger, T. Light Harvesting in Photosystem II Core Complexes Is Limited by the Transfer to the Trap: Can the Core Complex Turn into a Photoprotective Mode? *J. Am. Chem. Soc.* **2008**, *130*, 4431−4446.

(12) Renger, T.; Schlodder, E. Optical properties, excitation energy and primary charge transfer in photosystem II: theory meets experiment. *J. Photochem. Photobiol., B* **2011**, *104*, 126−141.

(13) Cardona, T.; Sedoud, A.; Cox, N.; Rutherford, A. W. Charge Separation in Photosystem II: A Comparative and Evolutionary Overview. *Biochim. Biophys. Acta, Bioenerg.* **2012**, *1817*, 26−43.

(14) Saito, K.; Ishida, T.; Sugiura, M.; Kawakami, K.; Umena, Y.; Kamiya, N.; Shen, J.-R.; Ishikita, H. Distribution of the Cationic State over the Chlorophyll Pair of the Photosystem II Reaction Center. *J. Am. Chem. Soc.* **2011**, *133*, 14379−14388.

(15) Narzi, D.; Bovi, D.; De Gaetano, P.; Guidoni, L. Dynamics of the special pair of chlorophylls of Photosystem II. *J. Am. Chem. Soc.* **2016**, *138*, 257−264.

(16) Müh, F.; Glöckner, C.; Hellmich, J.; Zouni, A. Light-induced quinone reduction in photosystem II. *Biochim. Biophys. Acta, Bioenerg.* **2012**, *1817*, 44−65.

(17) Reimers, J. R.; Biczysko, M.; Bruce, D.; Coker, D. F.; Frankcombe, T. J.; Hashimoto, H.; Hauer, J.; Jankowiak, R.; Kramer, T.; Linnanto, J.; Mamedov, F.; Müh, F.; Rätsep, M.; Renger, T.; Styring, S.; Wan, J.; Wang, Z.; Wang-Otomo, Z.-Y.; Weng, Y.-X.; Yang, C.; Zhang, J.-P.; Freiberg, A.; Krausz, E. Challenges facing an understanding of the nature of low-energy excited states in photosynthesis. *Biochim. Biophys. Acta, Bioenerg.* **2016**, *1857*, 1627−1640.

(18) Mamedov, M.; Nadtochenko, V.; Semenov, A. Primary electron transfer processes in photosynthetic reaction centers from oxygenic organisms. *Photosynth. Res.* **2015**, *125*, 51−63.

(19) Durrant, J. R.; Klug, D. R.; Kwa, S. L.; Van Grondelle, R.; Porter, G.; Dekker, J. P. A multimer model for P680, the primary electron donor of photosystem II. *Proc. Natl. Acad. Sci. U. S. A.* **1995**, *92*, 4798−4802.

(20) Raszewski, G.; Diner, B. A.; Schlodder, E.; Renger, T. Spectroscopic properties of reaction center pigments in photosystem II core complexes: revision of the multimer model. *Biophys. J.* **2008**, *95*, 105−119.

(21) Renger, T.; Schlodder, E. Primary photophysical processes in photosystem II: bridging the gap between crystal structure and optical spectra. *ChemPhysChem* **2010**, *11*, 1141−1153.

(22) Shibata, Y.; Nishi, S.; Kawakami, K.; Shen, J.-R.; Renger, T. Photosystem II does not possess a simple excitation energy funnel: time-resolved fluorescence spectroscopy meets theory. *J. Am. Chem. Soc.* **2013**, *135*, 6903−6914.

(23) Müh, F.; Plöckinger, M.; Renger, T. Electrostatic Asymmetry in the Reaction Center of Photosystem II. *J. Phys. Chem. Lett.* **2017**, *8*, 850−858.

(24) Deisenhofer, J.; Epp, O.; Miki, K.; Huber, R.; Michel, H. X-ray structure analysis of a membrane protein complex: Electron density map at 3 Å resolution and a model of the chromophores of the

photosynthetic reaction center from Rhodopseudomonas viridis. *J. Mol. Biol.* **1984**, *180*, 385−398.
(25) Woodbury, N. W.; Allen, J. P. In *Anoxygenic Photosynthetic Bacteria*; Springer: New York, 1995; pp 527−557.
(26) Romero, E.; Van Stokkum, I. H.; Novoderezhkin, V. I.; Dekker, J. P.; Van Grondelle, R. Two different charge separation pathways in photosystem II. *Biochemistry* **2010**, *49*, 4300−4307.
(27) Romero, E.; Novoderezhkin, V. I.; van Grondelle, R. Quantum design of photosynthesis for bio-inspired solar-energy conversion. *Nature* **2017**, *543*, 355−365.
(28) Nadtochenko, V.; Semenov, A. Y.; Shuvalov, V. Formation and decay of P680 $(P_{D1}-P_{D2})^+$ $Pheo_{D1}^-$ radical ion pair in photosystem II core complexes. *Biochim. Biophys. Acta, Bioenerg.* **2014**, *1837*, 1384−1388.
(29) Shelaev, I. V.; Gostev, F. E.; Vishnev, M. I.; Shkuropatov, A. Y.; Ptushenko, V. V.; Mamedov, M. D.; Sarkisov, O. M.; Nadtochenko, V. A.; Semenov, A. Y.; Shuvalov, V. A. P680 $(P_{D1}P_{D2})$ and Chl_{D1} as alternative electron donors in photosystem II core complexes and isolated reaction centers. *J. Photochem. Photobiol., B* **2011**, *104*, 44−50.
(30) Shelaev, I. V.; Gostev, F. E.; Nadtochenko, V. A.; Shkuropatov, A. Y.; Zabelin, A. A.; Mamedov, M. D.; Semenov, A. Y.; Sarkisov, O. M.; Shuvalov, V. A. Primary light-energy conversion in tetrameric chlorophyll structure of photosystem II and bacterial reaction centers: II. Femto- and picosecond charge separation in PSII D1/D2/Cyt b559 complex. *Photosynth. Res.* **2008**, *98*, 95.
(31) Groot, M. L.; Pawlowicz, N. P.; van Wilderen, L. J. G. W.; Breton, J.; van Stokkum, I. H. M.; van Grondelle, R. Initial electron donor and acceptor in isolated Photosystem II reaction centers identified with femtosecond mid-IR spectroscopy. *Proc. Natl. Acad. Sci. U. S. A.* **2005**, *102*, 13087−13092.
(32) Prokhorenko, V. I.; Holzwarth, A. R. Primary Processes and Structure of the Photosystem II Reaction Center: A Photon Echo Study. *J. Phys. Chem. B* **2000**, *104*, 11563−11578.
(33) Acharya, K.; Zazubovich, V.; Reppert, M.; Jankowiak, R. Primary electron donor (s) in isolated reaction center of photosystem II from *Chlamydomonas reinhardtii*. *J. Phys. Chem. B* **2012**, *116*, 4860−4870.
(34) Stewart, D. H.; Nixon, P. J.; Diner, B. A.; Brudvig, G. W. Assignment of the Q y absorbance bands of Photosystem II chromophores by low-temperature optical spectroscopy of wild-type and mutant reaction centers. *Biochemistry* **2000**, *39*, 14583−14594.
(35) Årsköld, S. P.; Masters, V. M.; Prince, B. J.; Smith, P. J.; Pace, R. J.; Krausz, E. Optical spectra of synechocystis and spinach photosystem II preparations at 1.7 K: identification of the D1-pheophytin energies and stark shifts. *J. Am. Chem. Soc.* **2003**, *125*, 13063−13074.
(36) Novoderezhkin, V. I.; Dekker, J. P.; Van Grondelle, R. Mixing of exciton and charge-transfer states in photosystem II reaction centers: modeling of stark spectra with modified redfield theory. *Biophys. J.* **2007**, *93*, 1293−1311.
(37) Romero, E.; Diner, B. A.; Nixon, P. J.; Coleman, W. J.; Dekker, J. P.; van Grondelle, R. Mixed exciton−charge-transfer states in photosystem II: stark spectroscopy on site-directed mutants. *Biophys. J.* **2012**, *103*, 185−194.
(38) Mokvist, F.; Sjöholm, J.; Mamedov, F.; Styring, S. The Photochemistry in Photosystem II at 5 K Is Different in Visible and Far-Red Light. *Biochemistry* **2014**, *53*, 4228−4238.
(39) Pavlou, A.; Jacques, J.; Ahmadova, N.; Mamedov, F.; Styring, S. The wavelength of the incident light determines the primary charge separation pathway in Photosystem II. *Sci. Rep.* **2018**, *8*, 2837.
(40) Thapper, A.; Mamedov, F.; Mokvist, F.; Hammarström, L.; Styring, S. Defining the far-red limit of photosystem II in spinach. *Plant Cell* **2009**, *21*, 2391−2401.
(41) Chen, M.; Blankenship, R. E. Expanding the solar spectrum used by photosynthesis. *Trends Plant Sci.* **2011**, *16*, 427−431.
(42) Wolf, B. M.; Blankenship, R. E. Far-red light acclimation in diverse oxygenic photosynthetic organisms. *Photosynth. Res.* **2019**, *142*, 349−359.
(43) Pettai, H.; Oja, V.; Freiberg, A.; Laisk, A. Photosynthetic activity of far-red light in green plants. *Biochim. Biophys. Acta, Bioenerg.* **2005**, *1708*, 311−321.
(44) Pettai, H.; Oja, V.; Freiberg, A.; Laisk, A. The long-wavelength limit of plant photosynthesis. *FEBS Lett.* **2005**, *579*, 4017−4019.
(45) Hughes, J. L.; Smith, P.; Pace, R.; Krausz, E. Charge separation in photosystem II core complexes induced by 690−730 nm excitation at 1.7 K. *Biochim. Biophys. Acta, Bioenerg.* **2006**, *1757*, 841−851.
(46) Greenbaum, N. L.; Mauzerall, D. Effect of irradiance level on distribution of chlorophylls between PS II and PS I as determined from optical cross-sections. *Biochim. Biophys. Acta, Bioenerg.* **1991**, *1057*, 195−207.
(47) Morton, J.; Akita, F.; Nakajima, Y.; Shen, J.-R.; Krausz, E. Optical identification of the long-wavelength (700−1700 nm) electronic excitations of the native reaction centre, Mn4CaO5 cluster and cytochromes of photosystem II in plants and cyanobacteria. *Biochim. Biophys. Acta, Bioenerg.* **2015**, *1847*, 153−161.
(48) Langley, J.; Morton, J.; Purchase, R.; Tian, L.; Shen, L.; Han, G.; Shen, J. R.; Krausz, E. The deep red state of photosystem II in Cyanidioschyzon merolae. *Photosynthetica* **2018**, *56*, 275−278.
(49) Nürnberg, D. J.; Morton, J.; Santabarbara, S.; Telfer, A.; Joliot, P.; Antonaru, L. A.; Ruban, A. V.; Cardona, T.; Krausz, E.; Boussac, A.; Fantuzzi, A.; Rutherford, A. W. Photochemistry beyond the red limit in chlorophyll f−containing photosystems. *Science* **2018**, *360*, 1210−1213.
(50) Mascoli, V.; Bersanini, L.; Croce, R. Far-red absorption and light-use efficiency trade-offs in chlorophyll *f* photosynthesis. *Nat. Plants* **2020**, *6*, 1044−1053.
(51) Danielius, R. V.; Satoh, K.; van Kan, P. J. M.; Plijter, J. J.; Nuijs, A. M.; van Gorkom, H. J. The primary reaction of photosystem II in the D1-D2-cytochrome b-559 complex. *FEBS Lett.* **1987**, *213*, 241−244.
(52) Mimuro, M.; Tomo, T.; Nishimura, Y.; Yamazaki, I.; Satoh, K. Identification of a photochemically inactive pheophytin molecule in the spinach D1-D2-cyt b559 complex. *Biochim. Biophys. Acta, Bioenerg.* **1995**, *1232*, 81−88.
(53) Montoya, G.; Yruela, I.; Picorel, R. Pigment stoichiometry of a newly isolated D1—D2—Cyt b_{559} complex from the higher plant *Beta vulgaris* L. *FEBS Lett.* **1991**, *283*, 255−258.
(54) Satoh, K.; Nakane, H. In *Current Research in Photosynthesis: Proceedings of the VIIIth International Conference on Photosynthesis Stockholm, Sweden, August 6−11, 1989*; Baltscheffsky, M., Ed.; Springer: Dordrecht, 1990; pp 271−274.
(55) Nanba, O.; Satoh, K. Isolation of a photosystem II reaction center consisting of D1 and D2 polypeptides and cytochrome b559. *Proc. Natl. Acad. Sci. U. S. A.* **1987**, *84*, 109−112.
(56) Novoderezhkin, V. I.; Romero, E.; Dekker, J. P.; van Grondelle, R. Multiple charge-separation pathways in photosystem II: modeling of transient absorption kinetics. *ChemPhysChem* **2011**, *12*, 681−688.
(57) Fuller, F. D.; Pan, J.; Gelzinis, A.; Butkus, V.; Senlik, S. S.; Wilcox, D. E.; Yocum, C. F.; Valkunas, L.; Abramavicius, D.; Ogilvie, J. P. Vibronic coherence in oxygenic photosynthesis. *Nat. Chem.* **2014**, *6*, 706−711.
(58) Duan, H.-G.; Prokhorenko, V. I.; Wientjes, E.; Croce, R.; Thorwart, M.; Miller, R. D. Primary charge separation in the Photosystem II reaction center revealed by a global analysis of the two-dimensional electronic spectra. *Sci. Rep.* **2017**, *7*, 12347.
(59) Krausz, E.; Cox, N.; Årsköld, S. P. Spectral characteristics of PS II reaction centres: as isolated preparations and when integral to PS II core complexes. *Photosynth. Res.* **2008**, *98*, 207−217.
(60) Hughes, J. L.; Prince, B. J.; Peterson Årsköld, S.; Smith, P. J.; Pace, R. J.; Riesen, H.; Krausz, E. The Native Reaction Centre of Photosystem II: A New Paradigm for P680. *Aust. J. Chem.* **2004**, *57*, 1179−1183.
(61) Sindra, P. Å.; Prince, B. J.; Krausz, E.; Smith, P. J.; Pace, R. J.; Picorel, R.; Seibert, M. Low-temperature spectroscopy of fully active PSII cores. Comparisons with CP43, CP47, D1/D2/cyt b559 fragments. *J. Lumin.* **2004**, *108*, 97−100.

https://dx.doi.org/10.1021/jacs.0c08526
J. Am. Chem. Soc. 2020, 142, 18174−18190

(62) Frankcombe, T. J. Explicit calculation of the excited electronic states of the photosystem II reaction centre. *Phys. Chem. Chem. Phys.* **2015**, *17*, 3295−3302.
(63) Ivashin, N.; Larsson, S. Excitonic states in photosystem II reaction center. *J. Phys. Chem. B* **2005**, *109*, 23051−23060.
(64) Vasil'ev, S.; Bruce, D. A protein dynamics study of photosystem II: the effects of protein conformation on reaction center function. *Biophys. J.* **2006**, *90*, 3062−3073.
(65) Suomivuori, C.-M.; Winter, N. O.; Hättig, C.; Sundholm, D.; Kaila, V. R. Exploring the Light-Capturing Properties of Photosynthetic Chlorophyll Clusters Using Large-Scale Correlated Calculations. *J. Chem. Theory Comput.* **2016**, *12*, 2644−2651.
(66) Gelzinis, A.; Abramavicius, D.; Ogilvie, J. P.; Valkunas, L. Spectroscopic properties of photosystem II reaction center revisited. *J. Chem. Phys.* **2017**, *147*, 115102.
(67) Zhang, L.; Silva, D.-A.; Zhang, H.; Yue, A.; Yan, Y.; Huang, X. Dynamic protein conformations preferentially drive energy transfer along the active chain of the photosystem II reaction centre. *Nat. Commun.* **2014**, *5*, 4170.
(68) Kitagawa, Y.; Matsuda, K.; Hasegawa, J.-y. Theoretical study of the excited states of the photosynthetic reaction center in photosystem II: Electronic structure, interactions, and their origin. *Biophys. Chem.* **2011**, *159*, 227−236.
(69) Palencar, P.; Prudnikova, T.; Vacha, F.; Kuty, M. The effects of light-induced reduction of the photosystem II reaction center. *J. Mol. Model.* **2009**, *15*, 923−933.
(70) Kawashima, K.; Ishikita, H. Energetic insights into two electron transfer pathways in light-driven energy-converting enzymes. *Chem. Sci.* **2018**, *9*, 4083−4092.
(71) König, C.; Neugebauer, J. Quantum Chemical Description of Absorption Properties and Excited-State Processes in Photosynthetic Systems. *ChemPhysChem* **2012**, *13*, 386−425.
(72) Thompson, M. A.; Zerner, M. C. A theoretical examination of the electronic structure and spectroscopy of the photosynthetic reaction center from *Rhodopseudomonas viridis*. *J. Am. Chem. Soc.* **1991**, *113*, 8210−8215.
(73) Parson, W. W.; Warshel, A. Spectroscopic properties of photosynthetic reaction centers. 2. Application of the theory to *Rhodopseudomonas viridis*. *J. Am. Chem. Soc.* **1987**, *109*, 6152−6163.
(74) Warshel, A.; Parson, W. W. Spectroscopic properties of photosynthetic reaction centers. 1. Theory. *J. Am. Chem. Soc.* **1987**, *109*, 6143−6152.
(75) Blomberg, M. R. A.; Siegbahn, P. E. M.; Babcock, G. T. Modeling Electron Transfer in Biochemistry: A Quantum Chemical Study of Charge Separation in *Rhodobacter sphaeroides* and Photosystem II. *J. Am. Chem. Soc.* **1998**, *120*, 8812−8824.
(76) Tamura, H.; Saito, K.; Ishikita, H. Acquirement of water-splitting ability and alteration of the charge-separation mechanism in photosynthetic reaction centers. *Proc. Natl. Acad. Sci. U. S. A.* **2020**, *117*, 16373−16382.
(77) Eisenmayer, T. J.; de Groot, H. J. M.; van de Wetering, E.; Neugebauer, J.; Buda, F. Mechanism and Reaction Coordinate of Directional Charge Separation in Bacterial Reaction Centers. *J. Phys. Chem. Lett.* **2012**, *3*, 694−697.
(78) Gelzinis, A.; Valkunas, L.; Fuller, F. D.; Ogilvie, J. P.; Mukamel, S.; Abramavicius, D. Tight-binding model of the photosystem II reaction center: application to two-dimensional electronic spectroscopy. *New J. Phys.* **2013**, *15*, 075013.
(79) Aksu, H.; Schubert, A.; Geva, E.; Dunietz, B. D. Explaining Spectral Asymmetries and Excitonic Characters of the Core Pigment Pairs in the Bacterial Reaction Center Using a Screened Range-Separated Hybrid Functional. *J. Phys. Chem. B* **2019**, *123*, 8970−8975.
(80) Aksu, H.; Schubert, A.; Bhandari, S.; Yamada, A.; Geva, E.; Dunietz, B. D. On the Role of the Special Pair in Photosystems as a Charge Transfer Rectifier. *J. Phys. Chem. B* **2020**, *124*, 1987−1994.
(81) Curutchet, C.; Mennucci, B. Quantum Chemical Studies of Light Harvesting. *Chem. Rev.* **2017**, *117*, 294−343.
(82) Artiukhin, D. G.; Eschenbach, P.; Neugebauer, J. Computational Investigation of the Spin-Density Asymmetry in Photosynthetic Reaction Center Models from First Principles. *J. Phys. Chem. B* **2020**, *124*, 4873−4888.
(83) Senn, H. M.; Thiel, W. QM/MM Methods for Biomolecular Systems. *Angew. Chem., Int. Ed.* **2009**, *48*, 1198−1229.
(84) Lin, H.; Truhlar, D. G. QM/MM: what have we learned, where are we, and where do we go from here? *Theor. Chem. Acc.* **2007**, *117*, 185−199.
(85) Mennucci, B. Modeling environment effects on spectroscopies through QM/classical models. *Phys. Chem. Chem. Phys.* **2013**, *15*, 6583−6594.
(86) Dreuw, A.; Harbach, P. H. P.; Mewes, J. M.; Wormit, M. Quantum chemical excited state calculations on pigment−protein complexes require thorough geometry re-optimization of experimental crystal structures. *Theor. Chem. Acc.* **2010**, *125*, 419−426.
(87) Wanko, M.; Hoffmann, M.; Strodel, P.; Koslowski, A.; Thiel, W.; Neese, F.; Frauenheim, T.; Elstner, M. Calculating Absorption Shifts for Retinal Proteins: Computational Challenges. *J. Phys. Chem. B* **2005**, *109*, 3606−3615.
(88) Dreuw, A.; Head-Gordon, M. Single-Reference ab Initio Methods for the Calculation of Excited States of Large Molecules. *Chem. Rev.* **2005**, *105*, 4009−4037.
(89) Dunietz, B. D.; Dreuw, A.; Head-Gordon, M. Initial Steps of the Photodissociation of the CO Ligated Heme Group. *J. Phys. Chem. B* **2003**, *107*, 5623−5629.
(90) Beglov, D.; Roux, B. An Integral Equation To Describe the Solvation of Polar Molecules in Liquid Water. *J. Phys. Chem. B* **1997**, *101*, 7821−7826.
(91) Imai, T.; Hiraoka, R.; Kovalenko, A.; Hirata, F. Locating missing water molecules in protein cavities by the three-dimensional reference interaction site model theory of molecular solvation. *Proteins: Struct., Funct., Genet.* **2007**, *66*, 804−813.
(92) Kovalenko, A.; Hirata, F. Three-dimensional density profiles of water in contact with a solute of arbitrary shape: a RISM approach. *Chem. Phys. Lett.* **1998**, *290*, 237−244.
(93) Sindhikara, D. J.; Hirata, F. Analysis of Biomolecular Solvation Sites by 3D-RISM Theory. *J. Phys. Chem. B* **2013**, *117*, 6718−6723.
(94) Sindhikara, D. J.; Yoshida, N.; Hirata, F. Placevent: An algorithm for prediction of explicit solvent atom distribution—Application to HIV-1 protease and F-ATP synthase. *J. Comput. Chem.* **2012**, *33*, 1536−1543.
(95) Schott-Verdugo, S.; Gohlke, H. PACKMOL-Memgen: A Simple-To-Use, Generalized Workflow for Membrane-Protein−Lipid-Bilayer System Building. *J. Chem. Inf. Model.* **2019**, *59*, 2522−2528.
(96) Martinez, L.; Andrade, R.; Birgin, E. G.; Martinez, J. M. PACKMOL: a package for building initial configurations for molecular dynamics simulations. *J. Comput. Chem.* **2009**, *30*, 2157−2164.
(97) Bayly, C. I.; Cieplak, P.; Cornell, W.; Kollman, P. A. A well-behaved electrostatic potential based method using charge restraints for deriving atomic charges: the RESP model. *J. Phys. Chem.* **1993**, *97*, 10269−10280.
(98) Duan, Y.; Wu, C.; Chowdhury, S.; Lee, M. C.; Xiong, G.; Zhang, W.; Yang, R.; Cieplak, P.; Luo, R.; Lee, T.; Caldwell, J.; Wang, J.; Kollman, P. A Point-Charge Force Field for Molecular Mechanics Simulations of Proteins Based on Condensed-Phase Quantum Mechanical Calculations. *J. Comput. Chem.* **2003**, *24*, 1999−2012.
(99) Becke, A. D. Density-Functional Thermochemistry. III. The Role Of Exact Exchange. *J. Chem. Phys.* **1993**, *98*, 5648−5652.
(100) Becke, A. D. A new mixing of Hartree−Fock and local density-functional theories. *J. Chem. Phys.* **1993**, *98*, 1372−1377.
(101) Sigfridsson, E.; Ryde, U. Comparison of methods for deriving atomic charges from the electrostatic potential and moments. *J. Comput. Chem.* **1998**, *19*, 377−395.
(102) Cornell, W. D.; Cieplak, P.; Bayly, C. I.; Gould, I. R.; Merz, K. M.; Ferguson, D. M.; Spellmeyer, D. C.; Fox, T.; Caldwell, J. W.; Kollman, P. A. A Second Generation Force Field for the Simulation of Proteins, Nucleic Acids, and Organic Molecules. *J. Am. Chem. Soc.* **1995**, *117*, 5179−5197.

https://dx.doi.org/10.1021/jacs.0c08526
J. Am. Chem. Soc. 2020, 142, 18174−18190

(103) Neese, F.; Wennmohs, F.; Becker, U.; Riplinger, C. The ORCA quantum chemistry program package. *J. Chem. Phys.* **2020**, *152*, 224108.
(104) Lu, T.; Chen, F. Multiwfn: A multifunctional wavefunction analyzer. *J. Comput. Chem.* **2012**, *33*, 580−592.
(105) Li, P.; Merz, K. M. Metal Ion Modeling Using Classical Mechanics. *Chem. Rev.* **2017**, *117*, 1564−1686.
(106) Ceccarelli, M.; Procacci, P.; Marchi, M. An ab initio force field for the cofactors of bacterial photosynthesis. *J. Comput. Chem.* **2003**, *24*, 129−142.
(107) Giammona, D. A. *Ph.D. Thesis*; University of California at Davis: Davis, CA, 1984.
(108) Sakashita, N.; Watanabe, H. C.; Ikeda, T.; Saito, K.; Ishikita, H. Origins of Water Molecules in the Photosystem II Crystal Structure. *Biochemistry* **2017**, *56*, 3049−3057.
(109) Guerra, F.; Siemers, M.; Mielack, C.; Bondar, A.-N. Dynamics of Long-Distance Hydrogen-Bond Networks in Photosystem II. *J. Phys. Chem. B* **2018**, *122*, 4625−4641.
(110) Maier, J. A.; Martinez, C.; Kasavajhala, K.; Wickstrom, L.; Hauser, K. E.; Simmerling, C. ff14SB: Improving the Accuracy of Protein Side Chain and Backbone Parameters from ff99SB. *J. Chem. Theory Comput.* **2015**, *11*, 3696−3713.
(111) Jorgensen, W. L.; Chandrasekhar, J.; Madura, J. D.; Impey, R. W.; Klein, M. L. Comparison of simple potential functions for simulating liquid water. *J. Chem. Phys.* **1983**, *79*, 926−935.
(112) Wang, J.; Wolf, R. M.; Caldwell, J. W.; Kollman, P. A.; Case, D. A. Development and testing of a general amber force field. *J. Comput. Chem.* **2004**, *25*, 1157−74.
(113) Dickson, C. J.; Madej, B. D.; Skjevik, Å. A.; Betz, R. M.; Teigen, K.; Gould, I. R.; Walker, R. C. Lipid14: The Amber Lipid Force Field. *J. Chem. Theory Comput.* **2014**, *10*, 865−879.
(114) Skjevik, Å. A.; Madej, B. D.; Walker, R. C.; Teigen, K. LIPID11: A Modular Framework for Lipid Simulations Using Amber. *J. Phys. Chem. B* **2012**, *116*, 11124−11136.
(115) Li, P.; Roberts, B. P.; Chakravorty, D. K.; Merz, K. M. Rational Design of Particle Mesh Ewald Compatible Lennard-Jones Parameters for + 2 Metal Cations in Explicit Solvent. *J. Chem. Theory Comput.* **2013**, *9*, 2733−2748.
(116) Li, P.; Song, L. F.; Merz, K. M. Parameterization of Highly Charged Metal Ions Using the 12−6-4 LJ-Type Nonbonded Model in Explicit Water. *J. Phys. Chem. B* **2015**, *119*, 883−895.
(117) Joung, I. S.; Cheatham, T. E. Molecular Dynamics Simulations of the Dynamic and Energetic Properties of Alkali and Halide Ions Using Water-Model-Specific Ion Parameters. *J. Phys. Chem. B* **2009**, *113*, 13279−13290.
(118) Joung, I. S.; Cheatham, T. E. Determination of Alkali and Halide Monovalent Ion Parameters for Use in Explicitly Solvated Biomolecular Simulations. *J. Phys. Chem. B* **2008**, *112*, 9020−9041.
(119) Loncharich, R. J.; Brooks, B. R.; Pastor, R. W. Langevin dynamics of peptides: The frictional dependence of isomerization rates of N-acetylalanyl-N′-methylamide. *Biopolymers* **1992**, *32*, 523−535.
(120) Ben-Shalom, I. Y.; Lin, C.; Kurtzman, T.; Walker, R. C.; Gilson, M. K. Simulating Water Exchange to Buried Binding Sites. *J. Chem. Theory Comput.* **2019**, *15*, 2684−2691.
(121) Berendsen, H. J. C.; Postma, J. P. M.; van Gunsteren, W. F.; DiNola, A.; Haak, J. R. Molecular dynamics with coupling to an external bath. *J. Chem. Phys.* **1984**, *81*, 3684−3690.
(122) Essmann, U.; Perera, L.; Berkowitz, M. L.; Darden, T.; Lee, H.; Pedersen, L. G. A Smooth Particle Mesh Ewald Method. *J. Chem. Phys.* **1995**, *103*, 8577−8593.
(123) Ryckaert, J.-P.; Ciccotti, G.; Berendsen, H. J. C. Numerical integration of the cartesian equations of motion of a system with constraints: molecular dynamics of *n*-alkanes. *J. Comput. Phys.* **1977**, *23*, 327−341.
(124) Götz, A. W.; Williamson, M. J.; Xu, D.; Poole, D.; Le Grand, S.; Walker, R. C. Routine Microsecond Molecular Dynamics Simulations with AMBER on GPUs. 1. Generalized Born. *J. Chem. Theory Comput.* **2012**, *8*, 1542−1555.
(125) Le Grand, S.; Götz, A. W.; Walker, R. C. SPFP: Speed without compromise—A mixed precision model for GPU accelerated molecular dynamics simulations. *Comput. Phys. Commun.* **2013**, *184*, 374−380.
(126) Salomon-Ferrer, R.; Götz, A. W.; Poole, D.; Le Grand, S.; Walker, R. C. Routine Microsecond Molecular Dynamics Simulations with AMBER on GPUs. 2. Explicit Solvent Particle Mesh Ewald. *J. Chem. Theory Comput.* **2013**, *9*, 3878−3888.
(127) Case, D. A.; Cheatham, T. E., III; Darden, T.; Gohlke, H.; Luo, R.; Merz, K. M., Jr.; Onufriev, A.; Simmerling, C.; Wang, B.; Woods, R. J. The Amber biomolecular simulation programs. *J. Comput. Chem.* **2005**, *26*, 1668−1688.
(128) Case, D. A.; Belfon, K.; Ben-Shalom, I. Y.; Brozell, S. R.; Cerutti, D. S.; Cheatham, T. E., III; Cruzeiro, V. W. D.; Darden, T. A.; Duke, R. E.; Ghoreishi, D.; Giambasu, G.; Giese, T.; Gilson, M .K.; Gohlke, H.; Goetz, A. W.; Greene, D.; Harris, R.; Homeyer, N.; Huang, Y.; Izadi, S.; Kovalenko, A.; Krasny, R.; Kurtzman, T.; Lee, T. S.; LeGrand, S.; Li, P.; Lin, C.; Liu, J.; Luchko, T.; Luo, R.; Man, V.; Mermelstein, D. J.; Merz, K. M.; Miao, Y.; Monard, G.; Nguyen, C.; Nguyen, H.; Onufriev, A.; Pan, F.; Qi, R.; Roe, D. R.; Roitberg, A.; Sagui, C.; Schott-Verdugo, S.; Shen, J.; Simmerling, C. L.; Smith, J.; Swails, J.; Walker, R. C.; Wang, J.; Wei, H.; Wilson, L.; Wolf, R. M.; Wu, X.; Xiao, L.; Xiong, Y.; York, D.M.; Kollman, P. A. *AMBER 2019*; University of California: San Francisco, 2019.
(129) Shao, J.; Tanner, S. W.; Thompson, N.; Cheatham, T. E. Clustering Molecular Dynamics Trajectories: 1. Characterizing the Performance of Different Clustering Algorithms. *J. Chem. Theory Comput.* **2007**, *3*, 2312−2334.
(130) Roe, D. R.; Cheatham, T. E., III Parallelization of CPPTRAJ enables large scale analysis of molecular dynamics trajectory data. *J. Comput. Chem.* **2018**, *39*, 2110−2117.
(131) Roe, D. R.; Cheatham, T. E. PTRAJ and CPPTRAJ: Software for Processing and Analysis of Molecular Dynamics Trajectory Data. *J. Chem. Theory Comput.* **2013**, *9*, 3084−3095.
(132) Metz, S.; Kästner, J.; Sokol, A. A.; Keal, T. W.; Sherwood, P. ChemShell—a modular software package for QM/MM simulations. *Wiley Interdiscip. Rev.: Comput. Mol. Sci.* **2014**, *4*, 101−110.
(133) Sherwood, P.; de Vries, A. H.; Guest, M. F.; Schreckenbach, G.; Catlow, C. R. A.; French, S. A.; Sokol, A. A.; Bromley, S. T.; Thiel, W.; Turner, A. J.; Billeter, S.; Terstegen, F.; Thiel, S.; Kendrick, J.; Rogers, S. C.; Casci, J.; Watson, M.; King, F.; Karlsen, E.; Sjøvoll, M.; Fahmi, A.; Schäfer, A.; Lennartz, C. QUASI: A general purpose implementation of the QM/MM approach and its application to problems in catalysis. *J. Mol. Struct.: THEOCHEM* **2003**, *632*, 1−28.
(134) Benediktsson, B.; Bjornsson, R. QM/MM Study of the Nitrogenase MoFe Protein Resting State: Broken-Symmetry States, Protonation States, and QM Region Convergence in the FeMoco Active Site. *Inorg. Chem.* **2017**, *56*, 13417−13429.
(135) Kästner, J.; Carr, J. M.; Keal, T. W.; Thiel, W.; Wander, A.; Sherwood, P. DL-FIND: An Open-Source Geometry Optimizer for Atomistic Simulations. *J. Phys. Chem. A* **2009**, *113*, 11856−11865.
(136) Ramos, F. C.; Nottoli, M.; Cupellini, L.; Mennucci, B. The molecular mechanisms of light adaption in light-harvesting complexes of purple bacteria revealed by a multiscale modeling. *Chem. Sci.* **2019**, *10*, 9650−9662.
(137) Bednarczyk, D.; Dym, O.; Prabahar, V.; Peleg, Y.; Pike, D. H.; Noy, D. Fine Tuning of Chlorophyll Spectra by Protein-Induced Ring Deformation. *Angew. Chem., Int. Ed.* **2016**, *55*, 6901−6905.
(138) Zucchelli, G.; Brogioli, D.; Casazza, A. P.; Garlaschi, F. M.; Jennings, R. C. Chlorophyll Ring Deformation Modulates Q_y Electronic Energy in Chlorophyll-Protein Complexes and Generates Spectral Forms. *Biophys. J.* **2007**, *93*, 2240−2254.
(139) Perdew, J. P.; Burke, K.; Ernzerhof, M. Generalized gradient approximation made simple. *Phys. Rev. Lett.* **1996**, *77*, 3865−3868.
(140) Weigend, F.; Ahlrichs, R. Balanced Basis Sets of Split Valence, Triple Zeta Valence and Quadruple Zeta Valence Quality for H to Rn: Design and Assessment of Accuracy. *Phys. Chem. Chem. Phys.* **2005**, *7*, 3297−3305.

https://dx.doi.org/10.1021/jacs.0c08526
J. Am. Chem. Soc. 2020, 142, 18174−18190

(141) Grimme, S.; Antony, J.; Ehrlich, S.; Krieg, H. A consistent and accurate ab initio parametrization of density functional dispersion correction (DFT-D) for the 94 elements H-Pu. *J. Chem. Phys.* **2010**, *132*, 154104.
(142) Grimme, S.; Ehrlich, S.; Goerigk, L. Effect of the Damping Function in Dispersion Corrected Density Functional Theory. *J. Comput. Chem.* **2011**, *32*, 1456−1465.
(143) Kendall, R. A.; Früchtl, H. A. The Impact of the Resolution of the Identity Approximate Integral Method on Modern ab Initio Algorithm Development. *Theor. Chem. Acc.* **1997**, *97*, 158−163.
(144) Sierka, M.; Hogekamp, A.; Ahlrichs, R. Fast Evaluation of the Coulomb Potential for Electron Densities Using Multipole Accelerated Resolution of Identity Approximation. *J. Chem. Phys.* **2003**, *118*, 9136−9148.
(145) Eichkorn, K.; Treutler, O.; Öhm, H.; Häser, M.; Ahlrichs, R. Auxiliary Basis Sets to Approximate Coulomb Potentials. *Chem. Phys. Lett.* **1995**, *240*, 283−290.
(146) Chai, J.-D.; Head-Gordon, M. Systematic optimization of long-range corrected hybrid density functionals. *J. Chem. Phys.* **2008**, *128*, 084106.
(147) Mardirossian, N.; Head-Gordon, M. ωB97X-V: A 10-parameter, range-separated hybrid, generalized gradient approximation density functional with nonlocal correlation, designed by a survival-of-the-fittest strategy. *Phys. Chem. Chem. Phys.* **2014**, *16*, 9904−9924.
(148) Najibi, A.; Goerigk, L. The Nonlocal Kernel in van der Waals Density Functionals as an Additive Correction: An Extensive Analysis with Special Emphasis on the B97M-V and ωB97M-V Approaches. *J. Chem. Theory Comput.* **2018**, *14*, 5725−5738.
(149) Cupellini, L.; Calvani, D.; Jacquemin, D.; Mennucci, B. Charge transfer from the carotenoid can quench chlorophyll excitation in antenna complexes of plants. *Nat. Commun.* **2020**, *11*, 662.
(150) Li, H.; Nieman, R.; Aquino, A. J. A.; Lischka, H.; Tretiak, S. Comparison of LC-TDDFT and ADC(2) Methods in Computations of Bright and Charge Transfer States in Stacked Oligothiophenes. *J. Chem. Theory Comput.* **2014**, *10*, 3280−3289.
(151) Izsák, R.; Neese, F. An overlap fitted chain of spheres exchange method. *J. Chem. Phys.* **2011**, *135*, 144105.
(152) Neese, F.; Wennmohs, F.; Hansen, A.; Becker, U. Efficient, Approximate and Parallel Hartree−Fock and Hybrid DFT Calculations. A 'Chain-of-Spheres' Algorithm for the Hartree−Fock Exchange. *Chem. Phys.* **2009**, *356*, 98−109.
(153) Tawada, Y.; Tsuneda, T.; Yanagisawa, S.; Yanai, T.; Hirao, K. A long-range-corrected time-dependent density functional theory. *J. Chem. Phys.* **2004**, *120*, 8425−8433.
(154) Cai, Z.-L.; Sendt, K.; Reimers, J. R. Failure of density-functional theory and time-dependent density-functional theory for large extended π systems. *J. Chem. Phys.* **2002**, *117*, 5543−5549.
(155) Dahlbom, M. G.; Reimers, J. R. Successes and failures of time-dependent density functional theory for the low-lying excited states of chlorophylls. *Mol. Phys.* **2005**, *103*, 1057−1065.
(156) Dreuw, A.; Head-Gordon, M. Failure of time-dependent density functional theory for long-range charge-transfer excited states: the zincbacteriochlorin−bacteriochlorin and bacteriochlorophyll−spheroidene complexes. *J. Am. Chem. Soc.* **2004**, *126*, 4007−4016.
(157) Neese, F. A critical evaluation of DFT, including time-dependent DFT, applied to bioinorganic chemistry. *JBIC, J. Biol. Inorg. Chem.* **2006**, *11*, 702−711.
(158) Linnanto, J.; Korppi-Tommola, J. Quantum chemical simulation of excited states of chlorophylls, bacteriochlorophylls and their complexes. *Phys. Chem. Chem. Phys.* **2006**, *8*, 663−687.
(159) Laurent, A. D.; Jacquemin, D. TD-DFT benchmarks: A review. *Int. J. Quantum Chem.* **2013**, *113*, 2019−2039.
(160) Loos, P.-F.; Scemama, A.; Jacquemin, D. The Quest for Highly Accurate Excitation Energies: A Computational Perspective. *J. Phys. Chem. Lett.* **2020**, *11*, 2374−2383.
(161) Shao, Y.; Mei, Y.; Sundholm, D.; Kaila, V. R. I. Benchmarking the Performance of Time-Dependent Density Functional Theory Methods on Biochromophores. *J. Chem. Theory Comput.* **2020**, *16*, 587−600.
(162) Eriksen, J. J.; Sauer, S. P. A.; Mikkelsen, K. V.; Christiansen, O.; Jensen, H. J. A.; Kongsted, J. Failures of TDDFT in describing the lowest intramolecular charge-transfer excitation in para-nitroaniline. *Mol. Phys.* **2013**, *111*, 1235−1248.
(163) Lischka, H.; Nachtigallová, D.; Aquino, A. J. A.; Szalay, P. G.; Plasser, F.; Machado, F. B. C.; Barbatti, M. Multireference Approaches for Excited States of Molecules. *Chem. Rev.* **2018**, *118*, 7293−7361.
(164) Izsák, R. Single-reference coupled cluster methods for computing excitation energies in large molecules: The efficiency and accuracy of approximations. *Wiley Interdiscip. Rev.: Comput. Mol. Sci.* **2020**, *10*, e1445.
(165) Dutta, A. K.; Neese, F.; Izsák, R. Towards a pair natural orbital coupled cluster method for excited states. *J. Chem. Phys.* **2016**, *145*, 034102.
(166) Dutta, A. K.; Nooijen, M.; Neese, F.; Izsák, R. Automatic active space selection for the similarity transformed equations of motion coupled cluster method. *J. Chem. Phys.* **2017**, *146*, 074103.
(167) Dutta, A. K.; Nooijen, M.; Neese, F.; Izsák, R. Exploring the Accuracy of a Low Scaling Similarity Transformed Equation of Motion Method for Vertical Excitation Energies. *J. Chem. Theory Comput.* **2018**, *14*, 72−91.
(168) Dutta, A. K.; Saitow, M.; Demoulin, B.; Neese, F.; Izsák, R. A domain-based local pair natural orbital implementation of the equation of motion coupled cluster method for electron attached states. *J. Chem. Phys.* **2019**, *150*, 164123.
(169) Dutta, A. K.; Saitow, M.; Riplinger, C.; Neese, F.; Izsák, R. A near-linear scaling equation of motion coupled cluster method for ionized states. *J. Chem. Phys.* **2018**, *148*, 244101.
(170) Riplinger, C.; Neese, F. An efficient and near linear scaling pair natural orbital based local coupled cluster method. *J. Chem. Phys.* **2013**, *138*, 034106.
(171) Sirohiwal, A.; Berraud-Pache, R.; Neese, F.; Izsák, R.; Pantazis, D. A. Accurate Computation of the Absorption Spectrum of Chlorophyll *a* with Pair Natural Orbital Coupled Cluster Methods. *J. Phys. Chem. B* **2020**, DOI: 10.1021/acs.jpcb.0c05761.
(172) Kozma, B.; Tajti, A.; Demoulin, B.; Izsák, R.; Nooijen, M.; Szalay, P. G. A New Benchmark Set for Excitation Energy of Charge Transfer States: Systematic Investigation of Coupled Cluster Type Methods. *J. Chem. Theory Comput.* **2020**, *16*, 4213−4225.
(173) Llansola-Portoles, M. J.; Li, F.; Xu, P.; Streckaite, S.; Ilioaia, C.; Yang, C.; Gall, A.; Pascal, A. A.; Croce, R.; Robert, B. Tuning antenna function through hydrogen bonds to chlorophyll *a*. *Biochim. Biophys. Acta, Bioenerg.* **2020**, *1861*, 148078.
(174) Agostini, A.; Meneghin, E.; Gewehr, L.; Pedron, D.; Palm, D. M.; Carbonera, D.; Paulsen, H.; Jaenicke, E.; Collini, E. How water-mediated hydrogen bonds affect chlorophyll a/b selectivity in Water-Soluble Chlorophyll Protein. *Sci. Rep.* **2019**, *9*, 1−10.
(175) Raszewski, G.; Saenger, W.; Renger, T. Theory of Optical Spectra of Photosystem II Reaction Centers: Location of the Triplet State and the Identity of the Primary Electron Donor. *Biophys. J.* **2005**, *88*, 986−998.
(176) Baker, N. A.; Sept, D.; Joseph, S.; Holst, M. J.; McCammon, J. A. Electrostatics of nanosystems: Application to microtubules and the ribosome. *Proc. Natl. Acad. Sci. U. S. A.* **2001**, *98*, 10037−10041.
(177) Zhang, M.; Bommer, M.; Chatterjee, R.; Hussein, R.; Yano, J.; Dau, H.; Kern, J.; Dobbek, H.; Zouni, A. Structural Insights into the Light-Driven Auto-Assembly Process of the Water-Oxidizing Mn_4CaO_5-Cluster in Photosystem II. *eLife* **2017**, *6*, e26933.
(178) Ahmadova, N.; Mamedov, F. Formation of Tyrosine Radicals in Photosystem II Under Far-Red Illumination. *Photosynth. Res.* **2018**, *136*, 93−106.
(179) Bao, H.; Burnap, R. L. Photoactivation: The Light-Driven Assembly of the Water Oxidation Complex of Photosystem II. *Front. Plant Sci.* **2016**, *7* DOI: 10.3389/fpls.2016.00578.
(180) Steffen, M. A.; Lao, K.; Boxer, S. G. Dielectric Asymmetry in the Photosynthetic Reaction Center. *Science* **1994**, *264*, 810−816.

(181) Saggu, M.; Fried, S. D.; Boxer, S. G. Local and Global Electric Field Asymmetry in Photosynthetic Reaction Centers. *J. Phys. Chem. B* **2019**, *123*, 1527−1536.
(182) Renger, T.; Müh, F. Understanding photosynthetic light-harvesting: a bottom up theoretical approach. *Phys. Chem. Chem. Phys.* **2013**, *15*, 3348−3371.
(183) Kavanagh, M. A.; Karlsson, J. K. G.; Colburn, J. D.; Barter, L. M. C.; Gould, I. R. A TDDFT investigation of the Photosystem II reaction center: Insights into the precursors to charge separation. *Proc. Natl. Acad. Sci. U. S. A.* **2020**, *117*, 19705.
(184) Niedringhaus, A.; Policht, V. R.; Sechrist, R.; Konar, A.; Laible, P. D.; Bocian, D. F.; Holten, D.; Kirmaier, C.; Ogilvie, J. P. Primary processes in the bacterial reaction center probed by two-dimensional electronic spectroscopy. *Proc. Natl. Acad. Sci. U. S. A.* **2018**, *115*, 3563−3568.
(185) Garcia-Ratés, M.; Neese, F. Effect of the Solute Cavity on the Solvation Energy and its Derivatives within the Framework of the Gaussian Charge Scheme. *J. Comput. Chem.* **2020**, *41*, 922−939.
(186) Cossi, M.; Rega, N.; Scalmani, G.; Barone, V. Energies, Structures, and Electronic Properties of Molecules in Solution with the C-PCM Solvation Model. *J. Comput. Chem.* **2003**, *24*, 669−681.
(187) Miyashita, H.; Ikemoto, H.; Kurano, N.; Adachi, K.; Chihara, M.; Miyachi, S. Chlorophyll *d* as a major pigment. *Nature* **1996**, *383*, 402−402.
(188) Chen, M.; Schliep, M.; Willows, R. D.; Cai, Z.-L.; Neilan, B. A.; Scheer, H. A Red-Shifted Chlorophyll. *Science* **2010**, *329*, 1318−1319.
(189) Renger, T.; Schlodder, E. The Primary Electron Donor of Photosystem II of the Cyanobacterium *Acaryochloris marina* Is a Chlorophyll *d* and the Water Oxidation Is Driven by a Chlorophyll *a*/Chlorophyll *d* Heterodimer. *J. Phys. Chem. B* **2008**, *112*, 7351−7354.
(190) Chen, M.; Telfer, A.; Lin, S.; Pascal, A.; Larkum, A. W.; Barber, J.; Blankenship, R. E. The nature of the photosystem II reaction centre in the chlorophyll d-containing prokaryote, *Acaryochloris marina*. *Photochem. Photobiol. Sci.* **2005**, *4*, 1060−1064.
(191) Judd, M.; Morton, J.; Nürnberg, D.; Fantuzzi, A.; Rutherford, A. W.; Purchase, R.; Cox, N.; Krausz, E. The primary donor of far-red photosystem II: Chl_{D1} or P_{D2}? *Biochim. Biophys. Acta, Bioenerg.* **2020**, *1861*, 148248.

https://dx.doi.org/10.1021/jacs.0c08526
J. Am. Chem. Soc. 2020, 142, 18174−18190